5-5-2017

The Orogenic Belt in Northern Taiwan: Is it Going Up or Down?

Han-Cheng Yu
han-cheng.yu@uconn.edu

The Orogenic Belt in Northern Taiwan: Is it Going Up or Down?

Han-Cheng Yu
B.S., Pennsylvania State University, 2014

A Thesis
Submitted in Partial Fulfillment of the
Requirements for the Degree of
Master of Science
At the
University of Connecticut
2017

APPROVAL PAGE

Master of Science Thesis

The Orogenic Belt in Northern Taiwan: Is it Going Up or Down?

Presented by
Han-Cheng Yu, B.S.

Major Advisor: _____
Timothy Byrne

Associate Advisor: _____
William Ouimet

Associate Advisor: _____
Jean Crespi

Associate Advisor: _____
Julie Fosdick

University of Connecticut
2017

ACKNOWLEDGMENTS

This work would not have been possible if it were not for the support from many individuals and institutions. I would first like to thank my outstanding advisors: Dr. Tim Byrne, Dr. William Ouimet, Dr. Jean Crespi, and Dr. Julie Fosdick. They were always willing to help me and guide me whenever I ran into a trouble spot or had a question about my research or writing. Without them, I won't be able to complete my research.

I would also like to thank the faculties, staff, and all the graduate students in Center of Integrative Geoscience. They welcomed me to be part of this science community and helped me with any problems related to school works in the last two years.

I would also like to thank the faculties and staff in Group 18 Laboratories at Arizona State University. They managed to find times for me to visit the laboratories and taught me to process zircon (U-Th)/He thermochronology. Without their help, I would never have data to support my research. I would also like to thank Prof. Yuan-Hsi Lee and his students in National Chung Cheng University. They were willing to set aside their works and taught me through all the processes about mineral separation and zircon fission track dating.

I would like to give special thanks to Wei-Hao Hsu, Chung Huang, Lindsey Belliveau, Ling-Ho Chung, and Queenie Chang. They gave me really big helps on my research and field works in Taiwan. Finally, I must express my very profound gratitude to my parents, my girlfriend (Felicity Hsu), my two cute dogs (Hardy and Emma), and all my friends with unfailing support and continuous encouragement throughout my years of study and through the process of researching. This accomplishment would not be possible without them. Thank you.

Table of Contents

CHAPTER ONE: INTRODUCTION

The obliquity between the north-south trending of Luzon arc and the northeast-southwest trending of Eurasian continental margin suggests a progression from collision to subduction and provides a time-for-space equivalence along strike. This propagating arc-continent collision model (Suppe, 1981) predicts that the initial collision began in northern Taiwan about 5-6 Ma and is just emerging above sea level in southern Taiwan. In addition, GPS-based velocity data and the progressive decrease in mean elevation from south to north suggests that the collision may be waning in the north. Extensional structures and earthquakes with normal fault focal mechanism in northern Taiwan have also been used as evidence for orogenic collapse during the waning stage of the collision (Teng, 1996). The Taiwan orogen, therefore, has been recognized as a textbook example of “the life of orogen” from subduction to collision to collapse. A recent earthquake along west-dipping Central Range fault (Chuang et al., 2014) and p-wave velocity tomography data (Wu et al, 2014) suggest, however, substantial shortening and possible subduction reversal in northern Taiwan. To better understand the tectonic setting of northern Taiwan, I present an age-elevation transect and thermal modeling of samples from Mt. Taiping based on new zircon (U-Th)/He and two zircon fission track ages. These new data are more consistent with rapid exhumation and orogenic growth rather than collapse. If collapse (i.e., a decrease in mean elevation) occurred in Mt. Taiping area, the age-elevation data suggest that it occurred after the youngest reset ZHe age or contemporaneously with exhumation.

CHAPTER TWO: BACKGROUND

2.1 Tectonic Settings and Models

The northern part of Taiwan island separates two subduction systems: The Luzon Arc system and the Ryukyu Arc system. The Luzon Arc system is on the south of Taiwan, where the South China Sea slab of the Chinese Continental Margin is eastward subducting underneath the Luzon Arc on the Philippine Sea plate. The Ryukyu system is on the east and northeast of Taiwan, where the Philippine Sea plate is subducting beneath the Eurasian plate along the Ryukyu trench. Both volcanic arcs extend on the island of Taiwan. The volcano groups found in northern Taiwan and northeastern offshore volcanic islands represents the westward extension of the Ryukyu arc. The Coastal Range on the eastern Taiwan is the northward extension of the Luzon volcanic arc.

The growth of Taiwan is a result of collision between the Eurasian plate and Philippine Sea plates. GPS measurements and the NUVEL-1 model of global plate motions show that the Philippine Sea plate is moving in a NW direction at a rate of 82 km/m.y. relative to the Eurasian plate (Yu et al., 1997). The obliquity between the northeast-southwest trending continental margin and the north-south trending Luzon volcanic arc provides a time for space equivalence of orogenic system (Figure 2). Southward-propagation model proposed by Suppe (1981,1984) has been the most widely accepted to describe the evolution of Taiwan mountain belt. The propagating model (Suppe, 1981, 1984; Teng, 1990) predicts that the initial collision began in northern Taiwan at about 5-6 Ma and is just emerging above sea level in southern

Taiwan. Calculated rates of southward-propagation range from 60 to 90 km/m.y. (Byrne and Liu, 2002; Suppe, 1984).

Numerous studies provide evidence in support the propagation model. The higher metamorphic grade rocks are exposed in northern Taiwan and decrease at the south (Stanley et al., 1981). Mélange is commonly considered to develop in the shallow structural levels of an accretionary prism. The Lichi mélange in the Longitudinal valley suture zone was developed when the Luzon arc-forearc was accreted to form the southern Central Range in the last 1 Ma (Huang et al., 2008). It suggests that the southern Taiwan is recently exhumed, which fits the propagation model (Teng and Wang, 1981; Teng et al., 1988). Finally, Quaternary erosion rates are higher in central and southern Taiwan and lowers in northern Taiwan (Dadson et al., 2003; Derrieux et al., 2014; Chen et al., 2015).

The compilation of seismic reflection data (Lin and Watts, 2002; Lin et al., 2003) and isopach maps from well data and field survey (Simoes and Avouac, 2006; Wu et al., 2011) suggests, however, rapid subsidence occurred at the same time in the north and south at 7 – 4 Ma (Lee et al., 2015). Hsu et al. (2016) complied low-temperature geochronology data and suggest three stages of accelerating cooling and exhumation throughout Central Range. Lee et al. (2015) suggest that the north-south trending Luzon arc collided with the north-south trending transitional continental crust at 5 Ma, which creates geologically simultaneous collision along strike (Figure 3).

2.2 Geological Background

The Taiwan orogenic belt is an active collision produced by the arc-continental collision of Luzon arc and Chinese continental margin. The belt can be divided into an accretionary prism west of the Longitudinal Valley with affinities related to Eurasia and a Coastal Range east of the valley which represents the collided Luzon arc. A fold-and-thrust belt is exposed in the Western Foothills and composed of Miocene pre-collisional continental margin sequence to Plio-Pleistocene syn-collisional foreland basin sequence (Teng, 1990). Sediment sequences in the Western Foothills also indicate that the foredeep evolved from an underfilled stage, characterized by a shift in environments from marine to terrestrial deposition and a relatively high rate of sediment (Simoes and Avouac, 2006). The Hsüehshan Range and the western Central Range expose two slate belts composed of Eocene to Miocene passive margin sediments (Ho, 1986) deformed into open to isoclinal folds that often verge westward. The Backbone Slate belt (the western Central Range) consists of two major stratigraphic units: the Miocene Lushan Formation and the Eocene Pilushan Formation. The Pilushan Formation is in direct contact with the overlying Miocene Lushan Formation, with no intervening Oligocene strata. The metamorphism grade is consistent across the two formations, suggesting that the unconformity is manly associated with depositional marine environment. In this oceanward part of the basin, Oligocene strata were either not deposited or were later eroded away. Sedimentation began again following marine transgression in late Oligocene or early Miocene time. Huang et al (1980a) stated that the Oligocene/Eocene unconformity is worldwide and is closely related to the overall lowering of sea level in Oligocene.

The Pilushan Formation forms a north-south trending belt along the eastern Central Range. The belt begins north at Suao near Ilan Plain and extends to Nantawushan in Pingtung in the south. The total length of the formation is nearly 250 kilometers and 1 – 5 kilometers wide (Ho, 1988). The formation is composed of slate and phyllite interbedded with thin to thick meta-sandstone and meta-conglomerate (Ho, 1988). The metamorphosed dark reddish volcanic rocks that are an important stratigraphic indicator are a minor lithologic component of the Pilushan Formation. The protoliths of meta-volcanic rocks are identified to be diabase and basaltic tuffaceous rocks (Tsan, 1977; Wu, 1978).

The age of the formation is dated to be in middle to late Eocene by foraminifers found in the matrix of the conglomerate (Lee and Lee, 1977). These fossils include *Nummulites* sp., *Assilina formosensis* Hanzawa, *Discocyclina* sp., and *Asterocyclina* sp (Lee and Lee, 1977; Chang and Hsu, 2011). These faunas were named the *Discocylina/Nummulites* zonule by Yabe and Hanzawa (1930). The distribution of fossils helps in mapping the area of the Pilushan Formation.

The Tananao complex is exposed in the eastern Central Range and is composed of green schist, black schist, and marble that is interpreted to represent pre-Tertiary Eurasian basement (Ho, 1986). Both the Tertiary cover sequences and the metamorphic basement have been subjected to multi-stage deformation and recrystallization due to different metamorphic events. The radiometric ages from igneous intrusion and metamorphism rocks using Rb-Sr, K-Ar, and U-Pb dating are suggesting that there are three major geological crustal evolution events results in several metamorphic events: 80-90 Ma Granitic intrusion in Taiwan; 35-40 Ma

Continental rifting and opening of South China Sea; 0-10 Ma Arc-continent collision (Juang and Bellon, 1986; Jahn et al., 1986; Tsao, 1996; Beyssac et al., 2007).

2.3 Low Temperature Thermochronology

There have been several thermochronology studies focusing on zircon fission track (ZFT) (Liu et al., 2001; Fuller et al., 2003; Lee et al., 2006; Fuller et al., 2006; Beyssac et al., 2007) and apatite fission track (AFT) (Liu, 1982; Willett et al., 2003; Fuller et al., 2006) in Taiwan since 1982. Nearly all of the ZFT and AFT ages come from Pliocene to Eocene sandstone and Tananao complex. Fuller et al (2006) distinguished the importance and the meaning of AFT and ZFT ages. Specifically, if the FT ages are older than the depositional age of its sedimentary host rock, the ages are interpreted as unreset or detrital. These ages show no relationship with the most recent collision process. In contrast, if the FT ages are younger than the stratigraphic age of the host rock, then the ages record varying degrees of post-depositional heating. Lastly, if the FT ages of a sample are all younger than depositional age of the host rock, then the sample has fully annealed and represents total reset and subsequent cooling associated with collisional or other exhumational processes. FT samples that exhibit partially annealed tracks provide added insights on the partial annealing zone and represents intermediate between a cooling age and the stratigraphic age. The distribution of reset AFT and ZFT is mainly located in Central Range and small fraction in Hsüehshan Range. The distribution of rest ages is similar to the distribution of green schist facies (Fuller et al., 2006; Lee et al., 2006), which provides insight for selecting study area for collecting reset age as cooling age.

Recently, there are two thermochronology studies focusing on zircon (U-Th)/He (Beyssac et al., 2007; Hsu et al., 2016). Beyssac et al. (2007) constructed a series of ZHe ages along Central Range and Hsüehshan Range to study the metamorphic evolution and exhumation of Taiwan mountain belt. Two transects of ZHe ages in the Tananao complex along Central Cross-Island Highway (CXIH) and Southern Cross-Island Highway (SXIH) show laterally constant patterns along strike. A series of ZHe dates show increasing ages from North to South in Hsüehshan Range, which suggests N-S progressive exhumation related to southward propagation. Hsu et al. (2016) compiled ZHe dates from Beyssac et al. (2007) and construct of two new ZHe ages transects. The four age-elevation transects are distributed near CXIH, SXIH, and Southern Taiwan in Central Range, and Mt. Yu in Hsüehshan Range. The exhumation rate is around 0.1 km/m.y. prior to 2 – 1.5 Ma; the rate is 2 - 4 km/m.y. between 2 – 1.5 Ma and 0.5 Ma; the rate is 4 – 8 km/m.y. from 0.5 Ma to present. Four transects suggest similar exhumation rate since 1 Ma, although onset of exhumation at Mt. Yu is slightly earlier than the rest of three transects. The earlier exhumation history at Mt. Yu may reflect displacement along a fault or shear zone between Central Range and Hsüehshan Range. The three age-elevation transects along Central Range provide insight to this study and are used to compare with the result in later section.

2.4 Low-Relief Topography

Low-relief areas as preserved relict topography are consistently found at high elevations near the main topographic divide of the Central Range. Low-relief surface could reflect an increase in rock uplift rate or a decrease in erosion rate, which interpreted in term of the history of uplift (Wipple et al., 2016). Cosmogenic radionuclide ^{10}Be from quartz suggests that low slope and low relief terrains exhibit a wide range of short-term erosion rates (0.1 to ~10 mm/yr) in Taiwan. Their existence in combination with constant, rapid background exhumation suggests that Taiwan has seen large-scale shifts in mean elevation over the last 2 Ma (Ouimet et al., 2015). Cueifong Lake in Mt. Taiping is recognized as a low relief surface in northern Central Range, which might provide an insight to this study and relate to exhumation history from new zircon (U-Th)/He and zircon fission track ages.

CHAPTER THREE: METHODS

3.1 (U-Th)/He Thermochronometry

The (U-Th)/He thermochronometer is based on the accumulation of ^{4}He in radioactive decay of Uranium, Thorium, and Samarium in minerals such as zircon and apatite (Wolf et al., 1996; Farley, 2002). When the rock/minerals are in high temperature environment above the effective closure temperature of that mineral, ^{4}He will instantly diffuse out of the system into the atmosphere or nearby crystals. Once the crystal has cooled to within the mineral's partial retention zone or below the effective closure temperature, the accumulation of ^{4}He will remain inside of the crystal. Thus, the concentrations of ^{4}He and the parent isotopes can be used to calculate a He date (Reiner and Brandon, 2006). Radiogenic ^{4}He will be retained in zircon at the closure temperature at 184 $\pm$ 13 ^{o}C, which represents the average temperature of the thermal window through which ^{4}He diffuses from zircon, termed the partial retention zone (Reiners et al. 2004). There are three primary factors that need to be considered in order to construct a well-constrained He date: U-Th rich inclusions, α-ejection, and radiation damage. During the handpicking process, zircon grains with no inclusions were selected for analysis to lower the uncertainty of the results. α-ejection is thought to occur in up to 10-30% of zircon and apatite grains depending on effective diffusion radius (Farley et al., 1996), which will lead to incorrect He dates and larger uncertainty. To correct for the ejection of α-particles, appropriate morphometric measurements of crystal dimensions are made to infer original crystal morphologies and calculate mass and effective radius. Radiation damage can potentially impact the closure temperature. The He retentivity of a grain, however, is a function of accumulated radiation damage in

the crystalline structure, which increases with time (Guenthner et al., 2013). Radiation damage is more common observed in older zircon grains (e.g., billions of years). For Taiwan, the radiation damage can be ignored due to zircon grains are relatively young (e.g., Mesozoic) and have low effective uranium concentrations.

3.2 Fission Track (FT) Dating

The fission track method measures the radiation damage produced by the radioactive decay of ^{238}U. The radiation damage is created by spontaneous fission of a single atom of ^{238}U that splits into two nuclei, that move through the crystal and damage the crystal lattice, forming a damage “track”. The track density is directly proportional to the time since the rock cooled below its annealing temperature; the age is calculated using the age equation discussed in Section 3.7.

The distribution of track lengths for a sample also provides additional insight for understanding the thermal history. Rezaeian (2008) illustrating different temperature histories relate to track length distribution. Although the fission track laboratory in National Chung Cheng University is not recording the track lengths for constructing the thermal history, with the rapid exhumation rate and short interval of time (0-5 Ma), the thermal history in Taiwan is corresponding to path 6, where rocks are heated into the partial annealing zone followed by rapid cooling to the surface.

3.3 Age-Elevation Transect Method

Mineral cooling histories are widely used to investigate long-term exhumation rates. Many techniques used to determine exhumation rates, however, require assuming a geothermal gradient. Interpretation of age-elevation transect data is a one-dimensional technique for estimating exhumation rate from thermochronometer ages without assuming a geothermal gradient. The elevation difference between samples with different cooling ages collected along a mountain slope can be used to estimate exhumation rates. In the age-elevation plot, the slope of best fit line through all the samples defines the apparent exhumation rate. Two important assumptions need to be considered in order for age-elevation profile to be accepted: 1) all rock samples follow a vertical exhumation path from the closure depth to the surface; 2) all the samples need to pass through the same closure isotherm with the same depth (Stuwe et al., 1994). The apparent exhumation rate derived from the profile will be valid when the assumptions are valid. The disadvantage of the method is that both local variations of topography and rock advection have the potential to affect the accuracy of apparent exhumation rate. Topography has a lateral cooling effect that may compress isotherms in the valleys and widen isotherms in the ridges, which create a spatial variation in the geothermal gradients (Mankcktelow and Graseman, 1997). Rapid rock advection or uplift will cause compression of isotherms, thereby affecting regional geothermal gradient and underestimate apparent exhumation rate (Stuwe et al., 1994).

3.4 Fieldwork

Taipingshan (Mt. Taiping) National Forest Recreation Area is located at Datong Township, Yilan. The recreation area is 13232 hectares and is mostly distributed in northern section of the Central Range, including Mt. Nanhu in the south and Mt. Sanshing in the center. The altitudes of the recreation area are between 500 – 2000 meters. The elevation of Taipingshan is approximately 1950 – 2000 m and Cueifong Lake is at 1850 – 2050 m. During the Japanese colonial period, the Taipingshan area was developed for the timber industry in 1915. In 1982, Forest Bureau closed the timbers field and transformed the area to Taipingshan National Forest Recreation Area. The recreation area now is famous for the historic sites from Japanese colonial period and natural mountainous landscapes with hot springs, snow, waterfalls and lakes.

The primary goal of the fieldwork was to collect rock samples near Mt. Taiping area in the northern Central Range. Mt (Figure 4). Taiping has been selected for the study due to its 2000 m elevation and located at the north peak of Central Range. Also, the mountain ranges in the Taipingshan Recreation Area have been suggested to be part of the collapsing belt (Teng, 1996). The recreation area also in the green schist facies, which suggests zircon fission track and (U-Th)/He thermochronometers are potentially totally reset. Each sample needs to be within in a limited distance with each other and with maximum slope between samples to create a near-vertical transect for fulfilling age-elevation profile assumption. Four samples were collected in the following elevations: 2031 m, 1800 m, 1500 m, and 1200 m. A fifth rock sample located at 1159 m from the same drainage basin was provided by Wei-Hao Hsu.

3.5 Mineral Separation

Mineral separation is the main procedure to extract zircon and apatite. Zircon and Apatite were separated from the bulk rock using well established methods. The first step is to crush the rock samples using a hammer into a suitable size for a grinder. The grinder crushes the samples into coarse to very fine grains. Using the different appropriate grain sieves to get the suitable grains that size in less than 300 μm. The sample was then washed and dried to remove dirt and mud material to prevent clinging between grains. Using the vibrating Gemini water table further separated the grains to heavy and light fractions. The heavy fraction of grains was then separated into magnetic and non-magnetic grains, using the Frantz magnetic separator by adjusting the power of the magnet in several runs. The nonmagnetic grains then undergo heavy liquid separation using lithium sodium tungstate (LST) liquid with a density of 2.85 g/mL to separate apatite/zircon at the bottom of the glass and other minerals floating on top of the liquid. Apatite and zircon can be separated from each other using methylene iodide with a density of 3.3 g/mL as the second heavy liquid separation. The zircon grains are denser than the liquid and will settle down to the bottom of the container. Apatite grains are lighter than the liquid and will float.

3.6 (U-Th)/He Analytical Procedure

Once the mineral separation is done, the zircon grains can be selected based on appropriate size, shape, clarity, and lack of inclusions. The zircon grains need to be in prismatic stubby or prismatic euhedral-needles shape with tetragonal prism widths of at least 75-90 μm (minimum of 60 μm). At least five grains from each sample are selected

and photographed. The dimensions of grains are measured in at least two mutually perpendicular perspectives parallel to the a_1 (long axis) and a_2 (short axis) crystallographic axes (Reiners, 2005). The dimensions measurements are used for α-ejection correction. Selected individual grains are packed into ~1 mm Pt/Nb foil envelope and place the packets into helium extraction line. The diode gas laser heating will extract helium gas and expand into a gas-source quadrupole mass spectrometer to measure $^4He/^3He$ ratio for the individual grains. After helium extraction, the grains are dissolved to measure concentration of U and Th using inductively coupled plasma-source mass spectrometry (ICPMS) (Reiners et al., 2002; Van Soest et al., 2011). (U-Th)/He dates can calculate from measurements and apply α-ejection correction to derive a corrected (U-Th)/He age (Farley et al., 1996; Hourigan et al., 2015). The procedure for this study was processed in Group 18 Laboratories at Arizona State University.

3.7 Zircon Fission Track Analytical Procedure

Once the mineral separation is done, the zircon grains can be selected under the criterion of large clear crystal. The zircon grains need to be in prismatic stubby or prismatic euhedral-needles shape, no crack surface, and no inclusions. Suitable zircon grains can be arranged one by one that all the grains are in one direction, and placed on a silica glass slide. The silica glass slide is then shifted onto a hot plate at a temperature of 315 °C (Hurford and Green, 1982). A sheet of 0.55 mm thick PFA Teflon covers on top of the glass slide and heated for 30 -60 sec. A second plate of silica glass is placed on top of the Teflon sheet and pressed gently so that the grains are fixed into

the Teflon sheet. Grinding and polishing the grains on the Teflon sheet will expose the flat internal surface for counting the tracks. After the grinding and polishing process, the chemical etching will make the tracks more visible under an optical microscope. For etching of zircon mounts, the Teflon sheet is placed into aluminum breaker containing NaOH:KOH with a ratio of 1:1 etchant. The required temperature of the etchant is 225 ± 1 °C (Murakami and Svojtka, 2007). Approximately a half day is necessary to finish the etching process for a typical batch of samples. After the etching process, all the Teflon sheets of grains from all the samples will be packed by two muscovite sheets as the external detectors and send it to National Tsing Hua University for thermal neutron irradiation. Once the samples are back from the thermal neutron irradiation, the fission track age can be calculated from the equation (Price and Walker, 1963; Naeser, 1967; Liu, 1982) below:

$$T = (\frac{1}{\lambda_d}) \times \ln\left[1 + \frac{\lambda_d \phi \sigma I \rho_s g}{\lambda_f \rho_i}\right]$$

Where

ρ_s = Density of natural spontaneous fission tracks.

ρ_I = Density of induced fission tracks (^{235}U) in a mica detector

λ_d = Total decay constant of ^{238}U (1.55125×10^{-10})

λ_f = Spontaneous fission decay constant for ^{238}U

I = Isotopic abundance ratio $^{235}U/^{238}U$ (7.252×10^{-3})

ϕ = neutron fluence, n/cm^{-2}

The fission track analysis for this study was processed in National Chung Cheng University.

3.8 HeFTy numerical modeling of thermal histories

The HeFTy program is developed by Dr. Richard Ketcham in University of Texas at Austin to interpret thermochronometric data (Ketcham, 2005). The program is name after a brand of trash bags as a reminder of the “garbage in, garbage out” principle. There are two ways of modeling in the program: forward modeling and inverse modeling. Forward modeling will predict thermochronology information based on the input of thermal history. Inverse modeling will predict thermal history based on the input of thermochronology data. This study uses inverse modeling of thermochronometric data. The Monte Carlo inversion algorithm of HeFTy program simulates the cooling history of rock materials from individual grains of sample and the detailed information about crystals. The information about crystal includes the radius of crystal, uncorrected or corrected (U-Th)/He date, and concentration of U and Th. The range of possible thermal histories was constrained by the depositional age of rock formation and a temperature window for peak metamorphism of the formation. The depositional age ranges from 34 to 38 Ma based on fossil records (Lee and Lee, 1977; Chang and Hsu, 2011) in the Eocene/Oligocene formation. Based on Raman spectroscopy of carbonaceous materials (Beyssac et al., 2007), the temperature window for peak metamorphism of these rocks ranges from 300 – 475 °C. Wintsch et al (2011) interpreted the peak metamorphism occurred less than 5 Ma. Each model of each sample is set to complete when the program determines there are 100 “good” goodness of fits (GOF). For each run, the program will determine different scenarios for “acceptable” GOF (>0.05) shown in green, “good” GOF (>0.5) shown in pink, and a weighted mean fit.

3.9 Estimation of exhumation rates

Bedrock exhumation rates are estimated using in three methods: exhumation rate equation (Liu, 1982); derived from HeFTy inverse modeling; and calculated from age-elevation profiles. The exhumation rate equation (Liu, 1982; Garver et al., 1999):

$$Exhumation\ rate = \frac{Cooling\ rate\ (℃/m.y.)}{geothermal\ gradient\ (℃/km)}$$

$$Cooling\ rate = \frac{T_c - T_s}{t}$$

where T_c is closure temperature, T_s is surface temperature, and t is timing of closure through T_c. The closure temperature for ZHe ranges from 171 to 196 °C (Reiner et al., 2004), and 184±13 °C is used for these calculations. The closure temperature for ZFT ranges from 205 to 265 °C (Bernet and Garver, 2005), and 235±30 °C is used in this study. The surface temperature is approximately 20 °C. Geothermal gradient used the modern thermal gradient which is approximately 55°C/km in the northern Central Range (Hsieh et al., 2014).

The second method is calculating the cooling rate using the slope change of weighted mean fit path in the temperature-time result derived from HeFTy inverse modeling. The “good” thermal paths from HeFTy were exported into Excel and derived the weight-mean paths for the last 5 Ma were extracted. The cooling rates were then divided by the modern thermal gradient (55°C/km) to derive the time-averaged exhumation rate.

The third method is estimating the apparent exhumation rate from age-elevation profile. The detailed procedures are described in age-elevation profile section.

CHAPTER FOUR: RESULT

4.1 Data

There were four samples collected and one sample provided by Wei-Hao Hsu, however, the sample TWTP-003 at elevation 1200m yielded insufficient zircon grain after mineral separation. After (U-Th)/He thermochronology dating, only samples TWTP-001 (1800 m) and Whe1129 (1129 m) had enough zircons to process for fission track dating. As result, there are four ZHe dates and two ZFT dates. Both methods show the ages of zircon grains are totally reset and younger than depositional age and can be interpreted as cooling ages. The ZFT ages range from 1.6 $\pm$ 0.3 Ma to 2.4 $\pm$ 0.2 Ma. The ZHe ages ranges from 0.73 $\pm$ 0.04 Ma to 0.99 $\pm$ 0.05 Ma (Table 1).

There are five grains dated for each sample and grain sizes were controlled during picking process. Variant grain sizes from one sample will increase the dissimilarity of uranium concentration, which may increase the uncertainty of sample age. All the grain sizes for each sample are selected and controlled in similar range. Thus, invariant grain sizes and uranium concentrations reduce the potential uncertainty for sample age.

An alpha particle ejection correction (Ft) was applied to (U-Th)/He dates of each grain calculated from the measurements to derive a corrected (U-Th)/He age of each grain (Farley et al., 1996; Hourigan et al., 2005). Each grain age was then calculated the outlier and weighted mean age calculation to determine the state of being excluded. The exclude grains were labeled in italic and underline in the Table 1 and each sample has at least three grains was pass the calculation successfully. The rest of grains was calculated inverse variance-weighted mean dates and the standard deviation of that weighted mean (σ_{WM}). The mean squared weighted deviation (MSWD) of the weighted

mean (Wendt and Carl, 1991) was also calculated for each sample. MSWD was a measure of the degree of dispersion of the data around the weighted mean. Three samples had sufficient magnitude of MSWD values indicate that the data scatter exceeded, which have larger uncertainties than the analytical uncertainties. An adjusted uncertainty ($\sigma_{WMadjusted}$) can derive from multiply σ_{WM} by the square-root of the MSWD to present more realistic uncertainties for three samples (Ludwig, 2003). In the table 1, $2\sigma_{WMadjusted}$ is reported for the uncertainties of TWTP-001, TWTP-004, and Whe1129.

CHAPTER FIVE: DISCUSSION

5.1 Age-Elevation Profile

This study reports data from a total of 10 samples from the study area/drainage basin: 4 ZHe, 2 ZFT, and 4 AFT (Liu, 1982). The elevations for all the samples used in the transect range from 150 m to 2031 m over a horizontal distance of 28 km. For one-dimensional age-elevation transect, the samples distribute throughout 28 km are not ideal for interpreting apparent exhumation rates. The relatively large dispersion, however, reflects only one outlier with most of the samples lying within a few kilometers of each other. Two age-elevation transects are constructed to solve the samples over-distributed throughout study area. For ZHe samples at 1500, 1800, and 2031m are located within limited distance of 3 km, which can be valid for the assumption that all the samples follow the same vertical path from the closure isotherm to the surface. The sample at elevation of 1129 m is located ~ 20 km away from the three samples although

in the same drainage basin. The cooling age of the sample at 1129 m, however, falls in the range of the apparent exhumation rate calculated from the three samples. Thus provides a great advantage to suggest the He-Ping drainage basin has the same exhumation history.

Similar situation for AFT samples, where CY-007 at elevation of 700 m is located further away from the rest of three AFT samples. The cooling age of sample CY-007, however, fits in the trend with the rest of samples and also suggests that the drainage basin has been exhuming together.

The regression fit of the Zircon FT ages predicts an apparent exhumation rate of 0.9 ± 0.1 km/myr; The Zircon He ages predicts an apparent exhumation rate of 3.4 ± 0.4 km/myr; the Apatite FT ages predicts an apparent exhumation rate of 10 ± 1.4 km/myr (Figure 6). The three low-temperature thermochronometry methods suggest increasing exhumation rate and cooling from 2.5 Ma to 0.3 Ma.

5.2 Zero-Age Intercept

Zero-age intercept extends the simple concept of age-elevation profile in one-dimensional model. The approach is to compare exhumation rate from the observed trend of age-elevation profile and the predicted closure depth using the modern geothermal gradient. The assumption for the zero-age intercept is that the modern thermal gradient is constant from the cooling ages to present or the isotherm is not affected by the change of topography. Also, the material path is passing through the closure temperature to surface vertically. Projected closure depth is determined by projecting the slope of age-elevation profile, the apparent exhumation rate, to zero to

estimate the closure depth. In northern Central Range, the modern thermal gradient is approximately 55 °C/km (Hsieh et al., 2014). Expected closure depth/elevation is calculated based on the modern thermal gradient in terms of the closure isotherm relative to the surface and mean elevation of the transect. The closure temperature range for zircon (U-Th)/He thermochronometer is 171 – 196 °C (Reiners et al., 2004) and the mean elevation for the transect is 1580 m. Assuming the thermal gradient at the mean elevation is 55 °C/km, the expected closure depth needs to be around 3000 - 3500 m below the mean elevation, which is about -1420 m to -1920 m. The comparison between the exhumation rate from projected slope of age-elevation profile and the exhumation rate from expected closure depth would be evidence that exhumation rate had increased/decreased after the ages of the samples. As the result, the zero-age intercepts show that the exhumation rates are similar, which suggests the exhumation rate is 3 - 4 km/myr and hasn't changed since 1 Ma (Figure 7).

5.3 HeFTy Modeling Results

Thermal paths from HeFTy modeling are exported into excel software to study "good" thermal path related to sample age and cooling history in the last 5 Ma. There are at least 100 "good" thermal paths and roughly 450 "acceptable" thermal paths on each HeFTy model result. The "good" thermal paths are used to calculate weighted mean path. The weighted mean path is used to estimate the cooling rate for last 3 Ma.

All the samples from HeFTy modeling shows accelerated cooling since around 3 Ma. The time-temperature history for TWTP-001 (1800m) with ZHe and ZFT ages shows the weighted mean fit path has two stages of accelerated cooling: the cooling

rate is 68 °C/m.y. from 2.5 Ma to 1 Ma and 196 °C/m.y. from 1 Ma to present. The modeling for WHe1129 (1129m) also show similar two stages of cooling history: the cooling rate is 68 °C/m.y. from 2.5 Ma to 1 Ma and 256 °C/m.y. from 1 Ma to present. The thermal history for TWTP-002 (1500m) and TWTP-004 (2031m), however, only show one stage of cooling history from 1.5 Ma to present at a rate of 188 °C/m.y. and 163 °C/m.y., respectively. Both models are lack of supported constraint relate to ZFT ages, which can only predict thermal paths only base on ZHe ages. The model results from each sample shows variation in the cooling rate that ranges from 163 °C/m.y. to 256 °C/m.y. from 1 Ma to present. The variation may relate to the samples ages, where younger age of a sample requires faster rate to arrive surface. The variation of cooling rate from HeFTy is consistent with the cooling rate calculation of each sample (table 3, 4), which suggest HeFTy modeling provides strong and robust result associate with ZHe and ZFT ages. Further exhumation rate derived from HeFTy is discussed in exhumation rates comparison section.

5.4 Comparison Among Estimated Exhumation Rates

The approach for exhumation rate calculations (table 3, 4 and figure 7) is to test consistency between different methods to further interpret the accuracy of exhumation rate for this study. The results from exhumation equation (Liu, 1982) show the exhumation rates for ZHe data ranges from 3.02 ± 0.28 km/m.y to 4.05 ± 0.39 km/m.y, with the weighted mean of 3.45 ± 0.38 km/m.y.. For ZFT, the exhumation rates range from 0.39 ± 0.32 km/m.y. to 0.59 ± 0.50 km/m.y., with average of 0.49 ± 0.41 km/m.y.. The HeFTy inverse modeling shows two stages of cooling path, which derives two

stages of exhumation rates: 1.24 km/m.y. from 2.5 Ma to 1Ma, and 2.96 to 4.65 km/m.y. with an average of 3.65 km/m.y. from 1 Ma to present. The apparent exhumation rate from the slope of age-elevation profile of ZHe and ZFT suggests 3.4 $\pm$ 0.4 km/m.y., and 0.9 $\pm$ 0.1 km/m.y., respectively.

The comparison shows the similarity in ZHe exhumation rates from three methods, which provides confidence on the accuracy of ZHe exhumation rate is approximately 3 – 4 km/m.y in the last 1 Ma. The ZFT exhumation rates, on the other hand, show variations between three methods. The range of ZFT and ZHe closure temperature results in larger uncertainty in exhumation rate derived from exhumation equation. Also, the exhumation rates derived from HeFTy cooling modeling are depended on the accuracy of assumed geothermal gradient.

CHAPTER SIX: CONCLUSION

Overall, four methods used to interpret ZHe and ZFT ages show consistent results and suggest two stages of exhumation in northern Central Range: relatively slow exhumation rates of ~ 1 km/m.y. from 2.5 Ma to 1 Ma and significantly faster exhumation rates of 3 – 4 km/m.y. from 1 Ma to present. The exhumation rates at Mt. Taiping from 1 Ma to the present are similar to rates documented by Hsu et al. (2016) for the central and southern sections of the Central Range, consistent with their hypothesis that the Central Range was exhumed simultaneously around 1 Ma.

The collapsing mountain belt hypothesis predicts that the topography in the Mt. Taiping area dropped from mean elevation of 3000 m to 2000 m, although other tectonic models are possible. Here I evaluate different models for the observed differences in elevation using the new exhumation cooling data and the age-elevation transect from the Central Cross-Island Hwy as a reference. The elevation offset between the study area (2000m) and CXIH (3000m) could be related to: 1) “collapse” of the mountain topography as the orogeny propagates from north to south; 2) differential uplift and exhumation from north to south before 1 Ma. or 3) differential uplift and exhumation from north to south after 0.7 Ma. (Figure 20)

Based on southward propagation model in which both orogenic uplift and collapse propagate southward, the Mt. Taiping area would be predicted to uplifted to 3000 m before the CXIH area. This difference in initial uplift would therefore be recorded in a slightly older onset of exhumation in the north relative to CXIH. However, the ZHe age transects in both Mt. Taiping and the CXIH are similar, suggesting that they followed similar exhumation histories. Thus, the exhumation history from both age transects are

inconsistent with the hypothesis of the collapsing mountain belt associated with southward propagation.

A second possibility is that before 1 Ma, the Mt. Taiping area was undergoing slower exhumation than the CXIH area. The ZFT data, which records the exhumation history prior to 1 Ma (Figure 19), suggests a slightly higher exhumation rate in the CXIH area compared to the Mt Taiping. However, the data points for from the CXIH are scattered and the associated error bars are relatively large. In addition, only two ages constrain the exhumation history from the Mt Taiping area. Thus, the slightly higher exhumation from the CXIH between 2.5 and 1 Ma is poorly constrained. The ZHe data shows that between 1 Ma and about 0.7 Ma (and presumably to the Present) Mt Taiping and CXIH had similar exhumation histories. The observed offset in topography may therefore be a remnant of different exhumation histories prior to ~1 Ma (Figure 20A).

A third possibility is that differential exhumation between the two sites occurred after 0.7 Ma. That is, uplift of the CXIH area or subsidence of the Mt. Taiping area since 0.7 Ma may explain the offset in topography. This interpretation predicts that the cooling paths recorded in the rocks prior to 0.7 Ma in each area would also be offset ~1000 m. and this prediction can be evaluated with the ZHe data from the two areas. Figure 18 shows that although the ZHe data from the two areas allow for the possible offset, the scatter in the ages and their errors also allow for no offset (Figure 20B).

Finally, Ouimet et al. (2015) have proposed that the topography records incision into a preexisting elevated low-relief surfaces have been interpreted the history of rock uplift. If the low relief surfaces correlated with each other and have relatively young age (<1 Ma), these could suggest the offset occurred after 1 Ma.

FIGURES

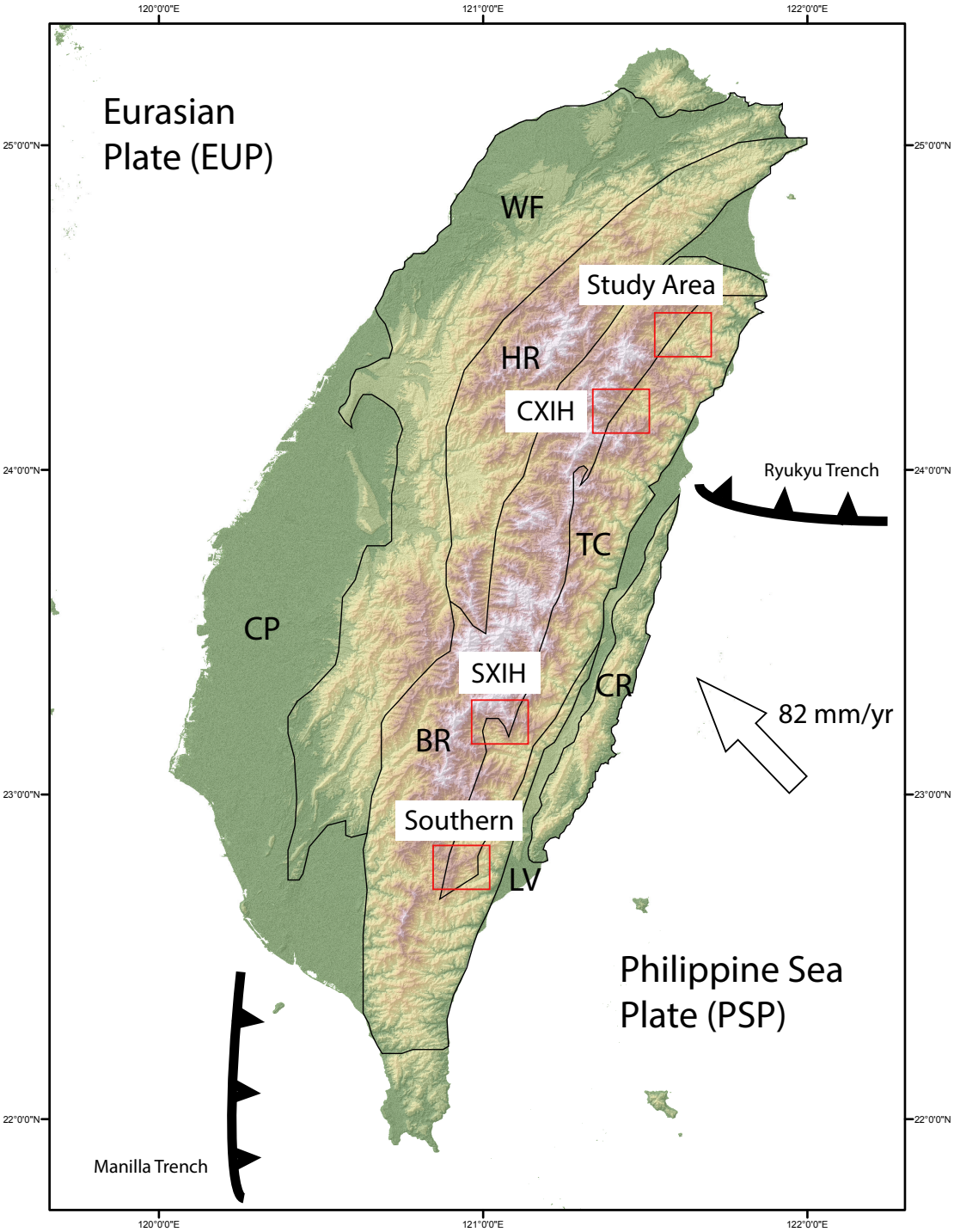

Figure 1. Tectonic and geologic settings of Taiwan. CP – Coastal Plain; WF – Western Foothills; HR - Hsüehshan Range; BR – Backbone Range (Western Central Range); TC – Tananao Complex (Eastern Central Range); LV – Longitudinal Valley; CR – Coastal Range. Red boxes represent four locations of the age-elevation transects: northern Taiwan from this study; Central Cross-Island Highway, Southern Cross-Island Highway, and southern Taiwan from Hsu et al. (2016).

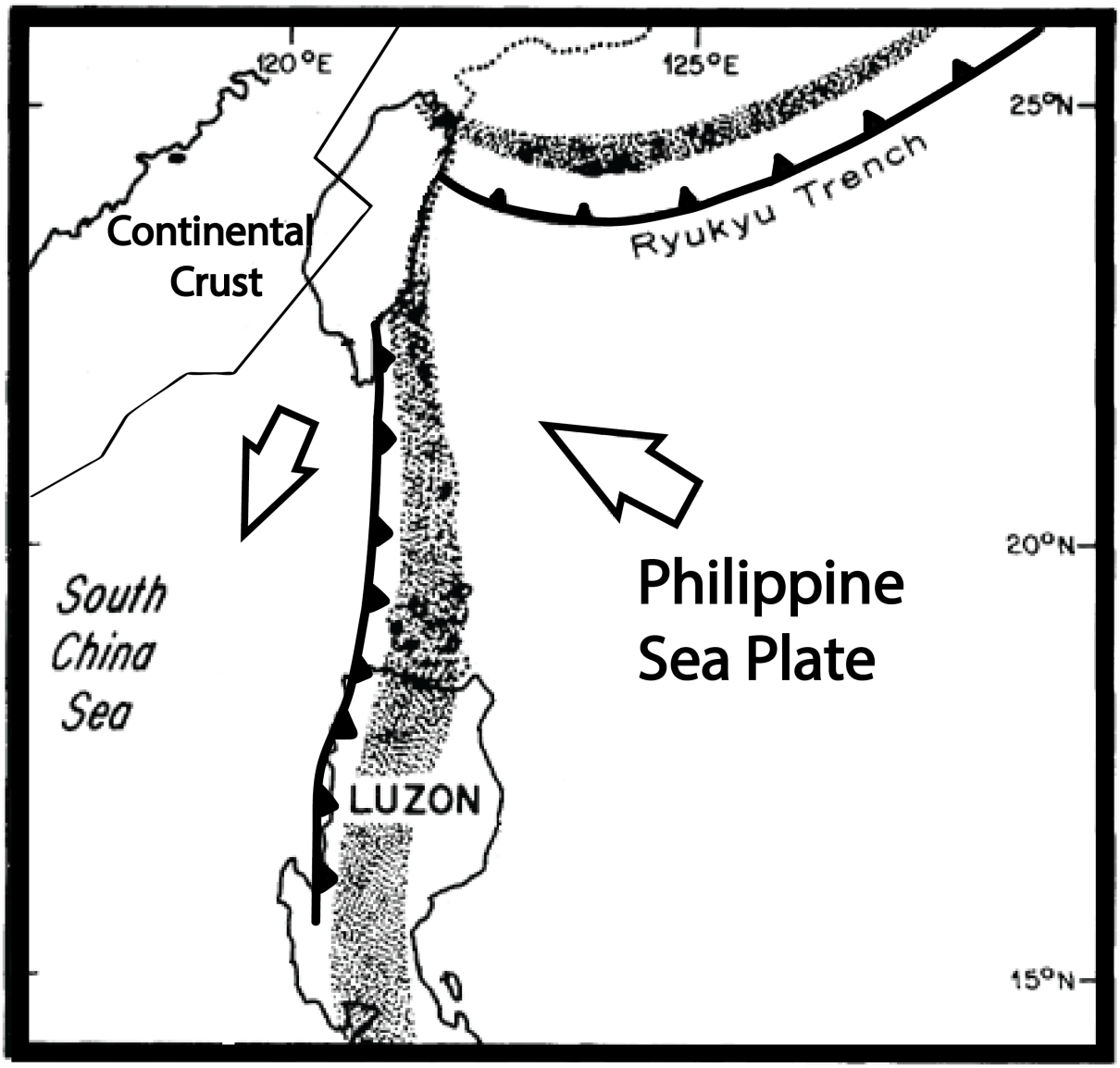

Figure 2. A tectonic map shows the obliquity of Philippine Sea Plate relative to continental margin provides a time for space equivalence of orogenic system. The propagating model (Suppe, 1981, 1984; Teng, 1990) predicts that the initial collision began in northern Taiwan at about 5-6 Ma and is just emerging above sea level in southern Taiwan.

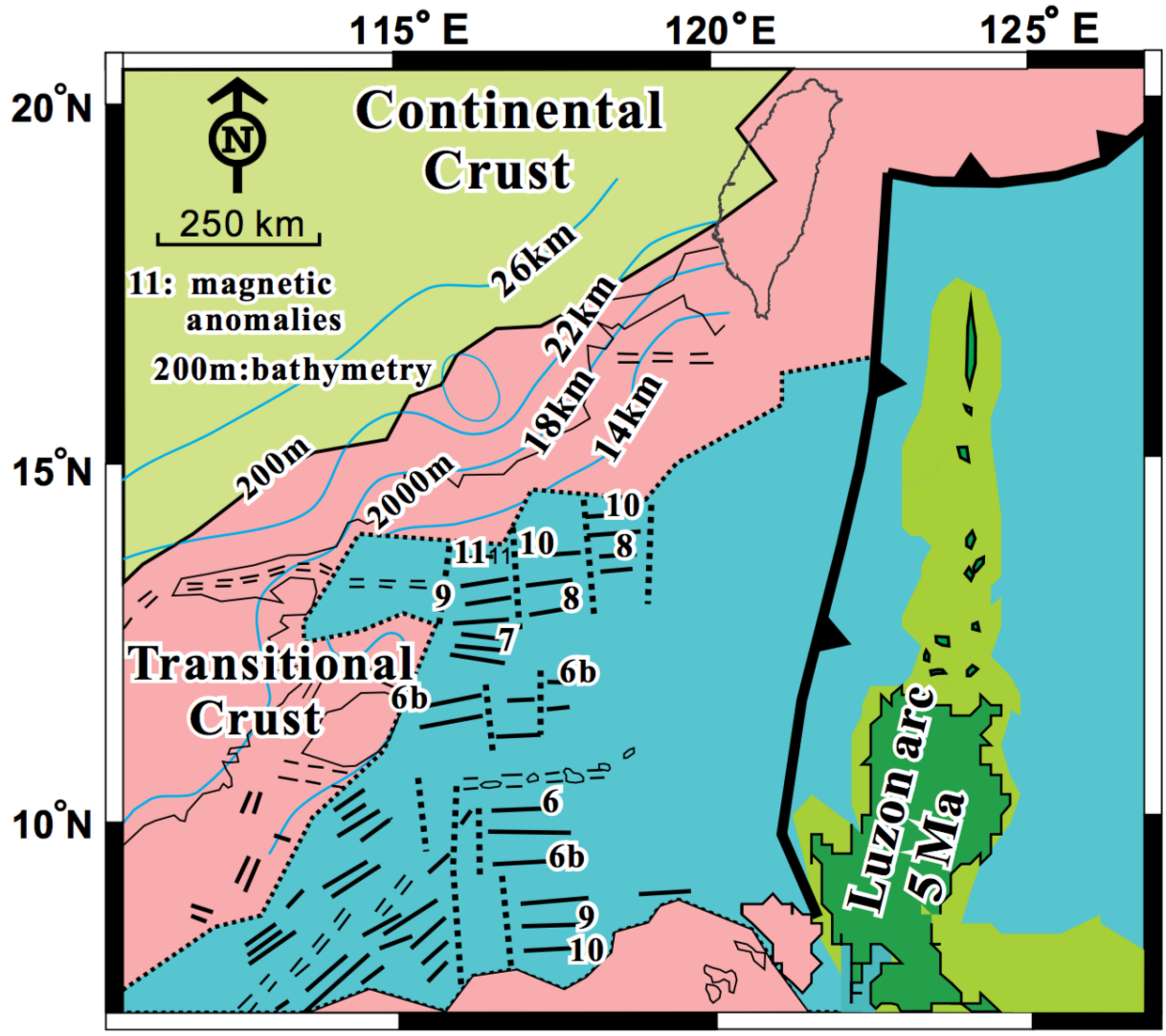

Figure 3. A tectonic plate map shows a wide zone of north-south trending transitional crust collided with the north-south trending Luzon arc that produces a collision occurred simultaneously along strike of Taiwan island (from Lee et al., 2015).

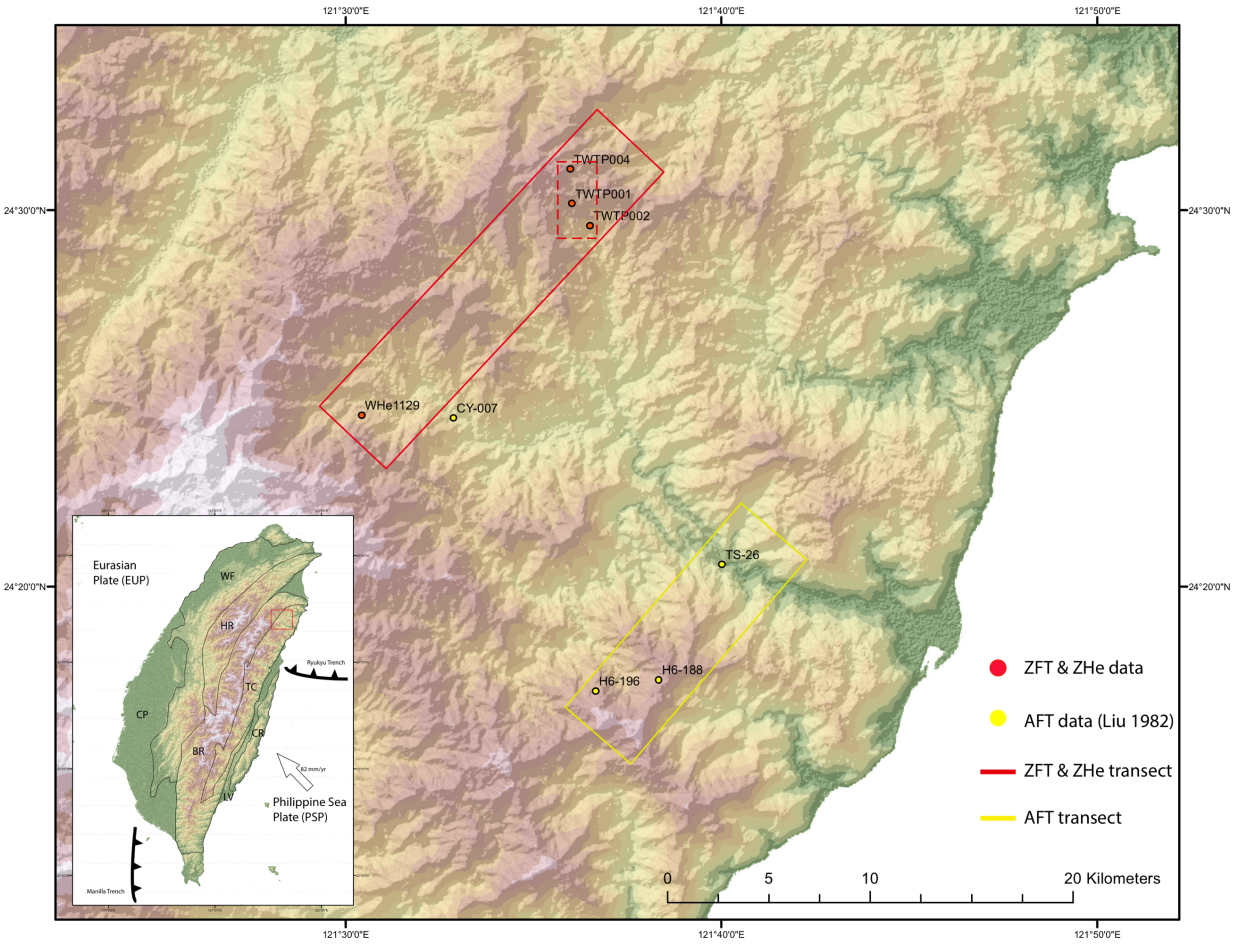

Figure 4. Location map of study area. Red dots – samples collected for ZHe and ZFT thermochronometry dating; Yellow dots – AFT samples from Liu (1982); Red box – the age-elevation transect for ZHe and ZFT; Yellow box and CY-007 – the age elevation transect for AFT.

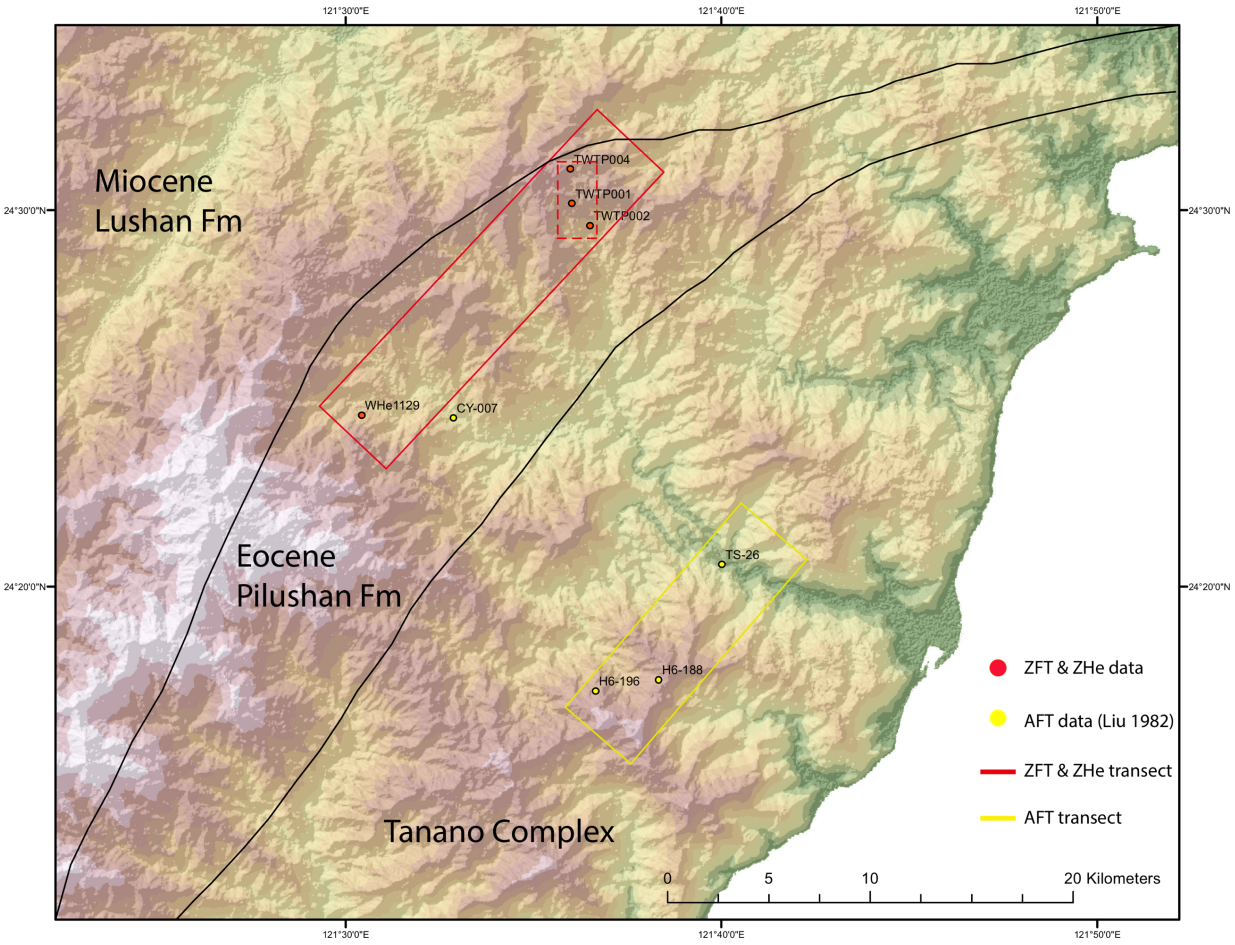

Figure 5. Geologic and topographic relief maps of the study area. ZHe and ZFT samples collected in Eocene Pilushan Formation that is part of Backbone Range. AFT samples are from Tananao Complex. Both Formations have been subjected to multi-stage deformation and recrystallization due to different metamorphic events.

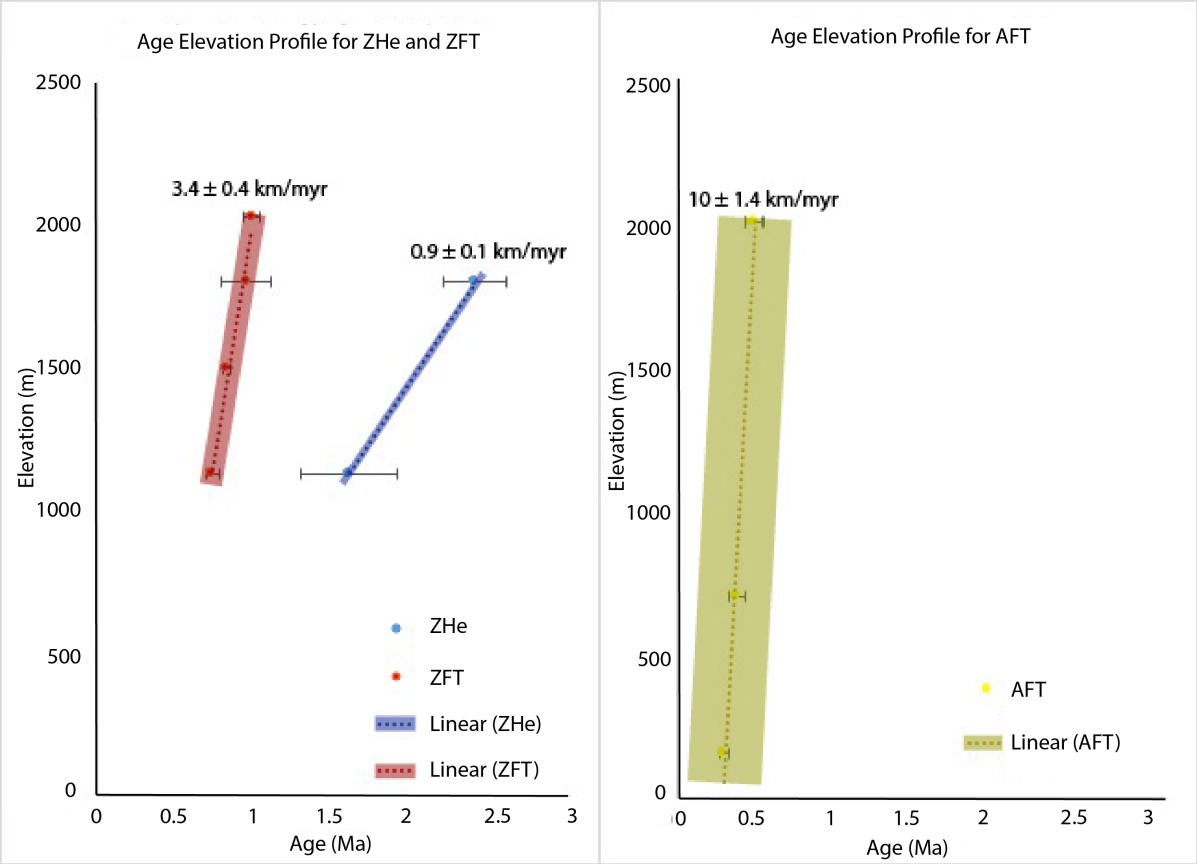

Figure 6. Age-elevation profiles for three thermochronometers. Blue dot – ZFT data; Red dot – ZHe data; Yellow dot – AFT data; Blue line – Best fit of ZFT; Red line – Best fit of ZHe; Yellow line – Best fit of AFT. The thickness of color bar is correlated with uncertainty of apparent exhumation rate.

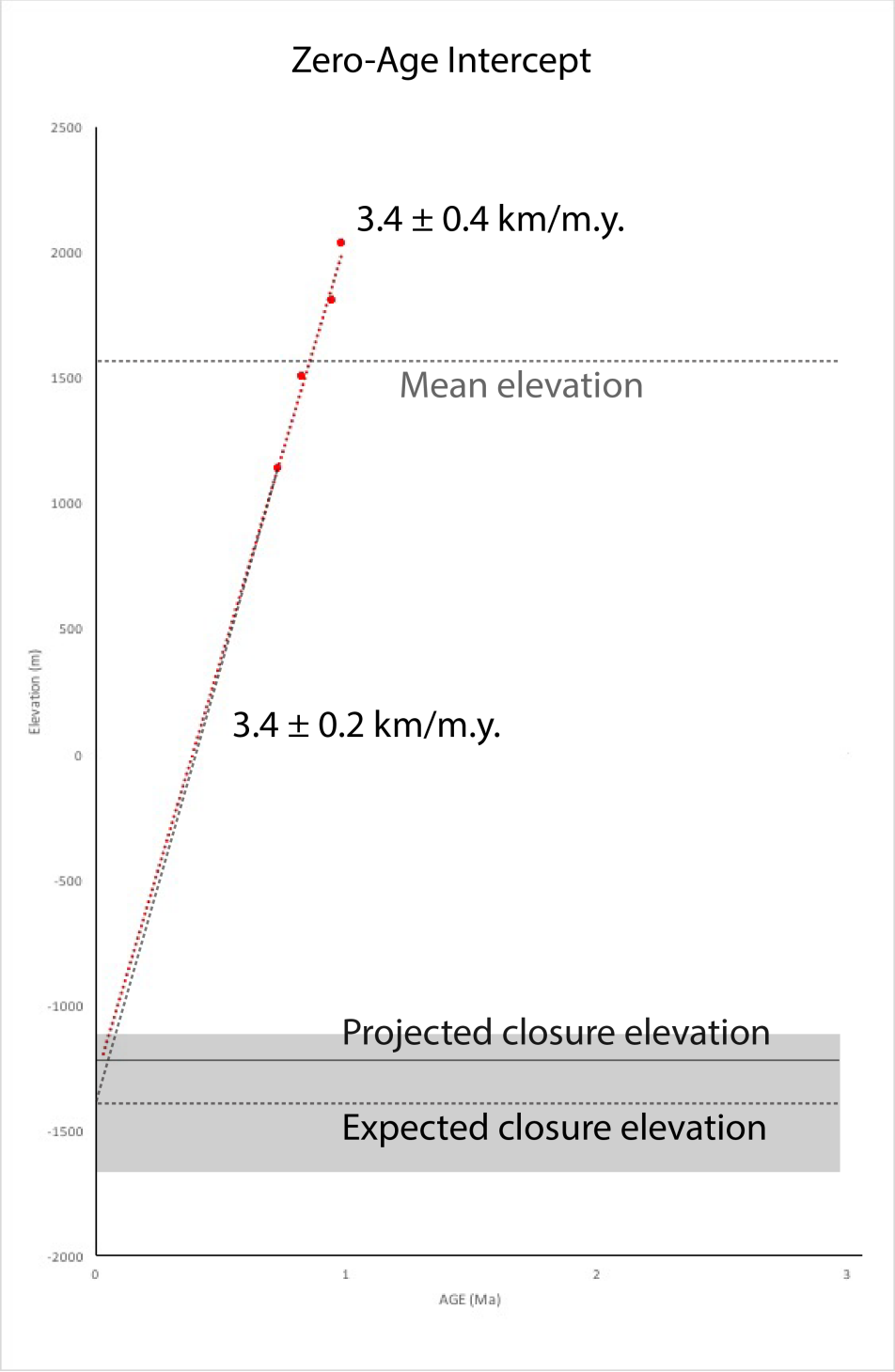

Figure 7. The zero-age intercept for (U-Th)/He ages. Grey Area – expected closure depth ranges. 1) expected closure depth beneath the present mean elevation estimated by the modern thermal gradient and 2) projected closure depth assuming no change on exhumation rate since about 1 Ma (time of closure for rocks at the mean elevation) respectively. Both projected and expected trends are similar pattern, which suggests the exhumation rate and the modern thermal gradient haven't change since 1 Ma.

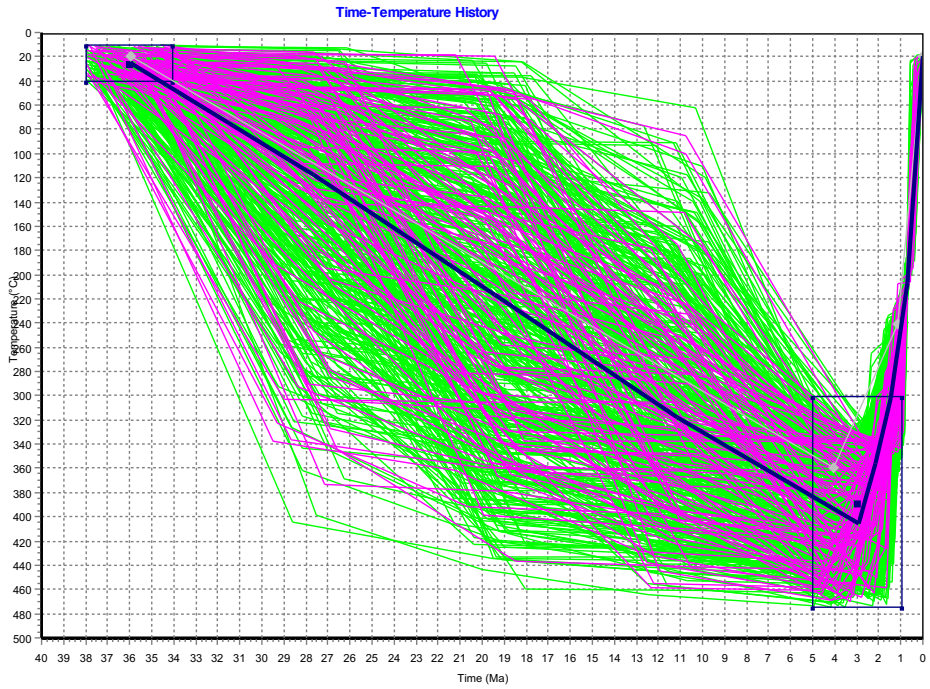

Figure 8. HeFTy Time-temperature model result of ZHe and ZFT for WHe1129 at elevation of 1129m.

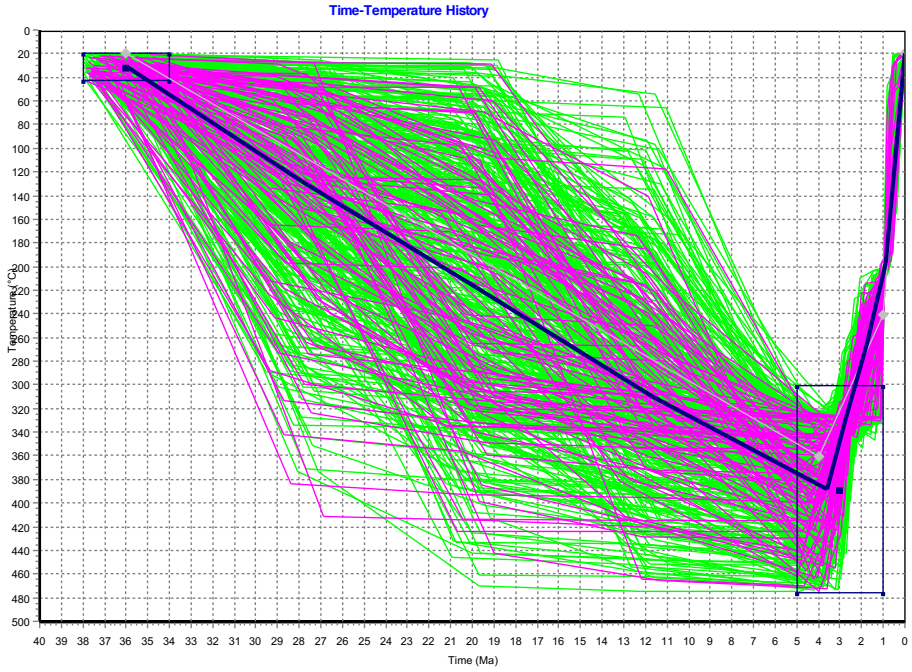

Figure 9. HeFTy Time-temperature model result of ZHe and ZFT for TWTP-001 at elevation of 1800 m.

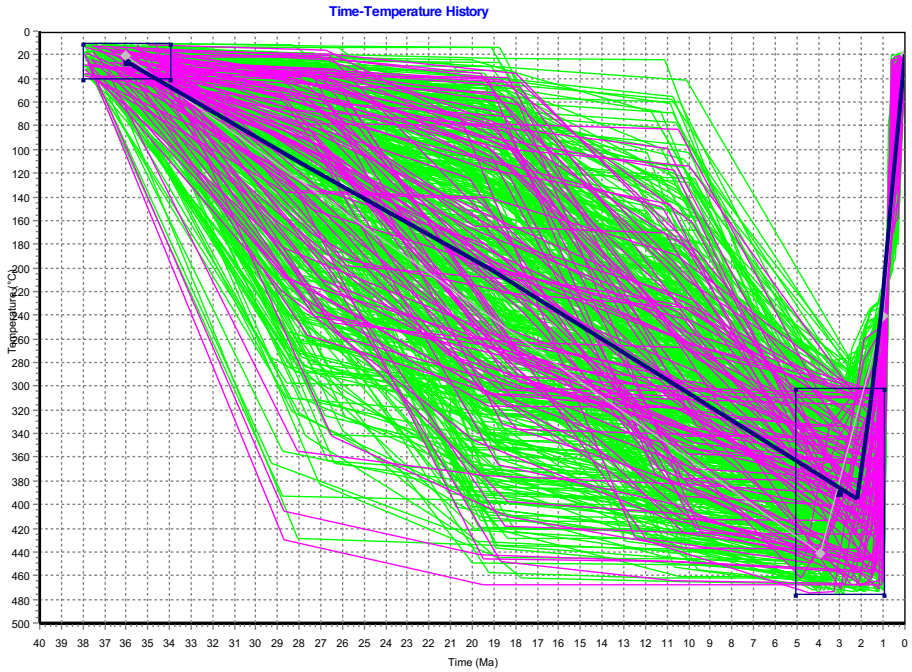

Figure 10. HeFTy Time-temperature model result of ZHe for TWTP-002 at elevation of 1500m.

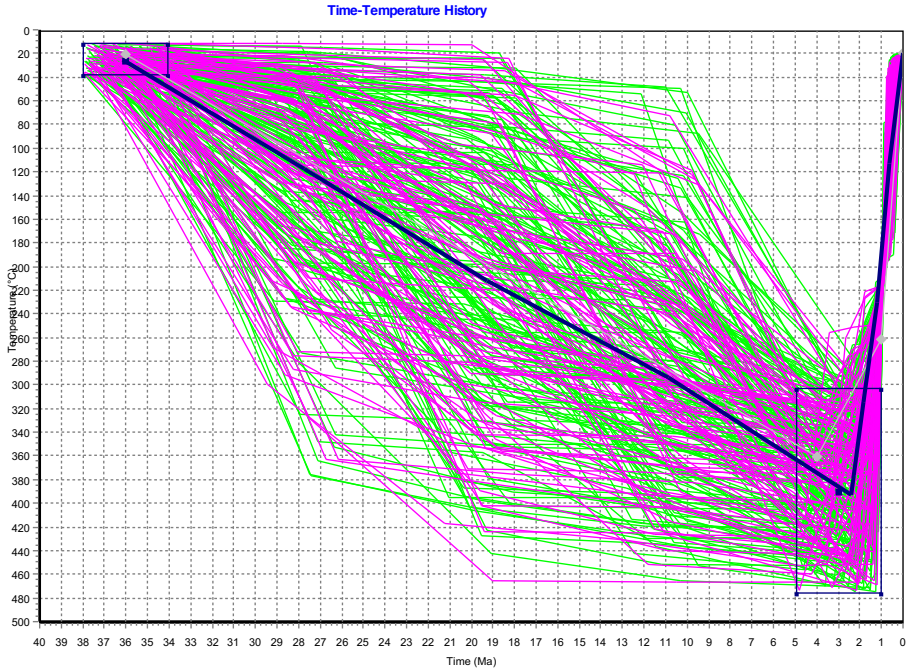

Figure 11. HeFTy Time-temperature model result of ZHe for TWTP-004 at elevation of 2031m.

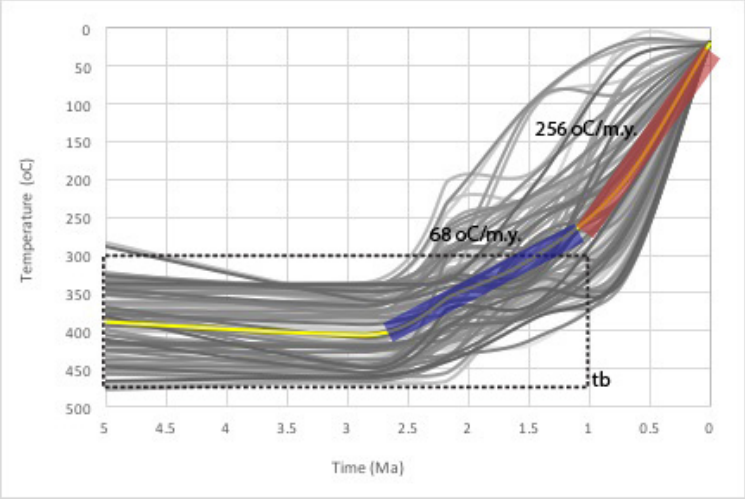

Figure 12. Time-temperature model result of ZHe and ZFT for WHe1129 at elevation of 1129m. The model focuses on two stages of accelerating cooling history in the last 2.5 Ma. The cooling rates are 68 °C/m.y. from 2.5 Ma to 1 Ma, and 256 °C/m.y. from 1 Ma to present.

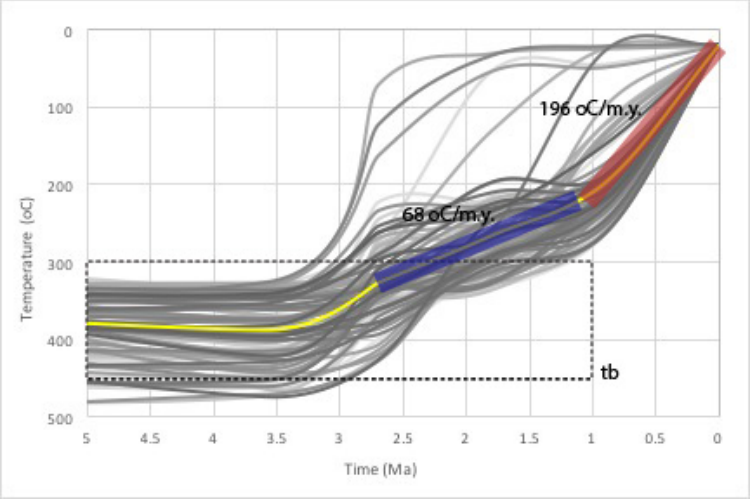

Figure 13. Time-temperature model result of ZHe and ZFT for TWTP-001 at elevation of 1800m. The model focuses on two stages of accelerating cooling history in the last 2.5 Ma. The cooling rates are 68 °C/m.y. from 2.5 Ma to 1 Ma, and 196 °C/m.y. from 1 Ma to present.

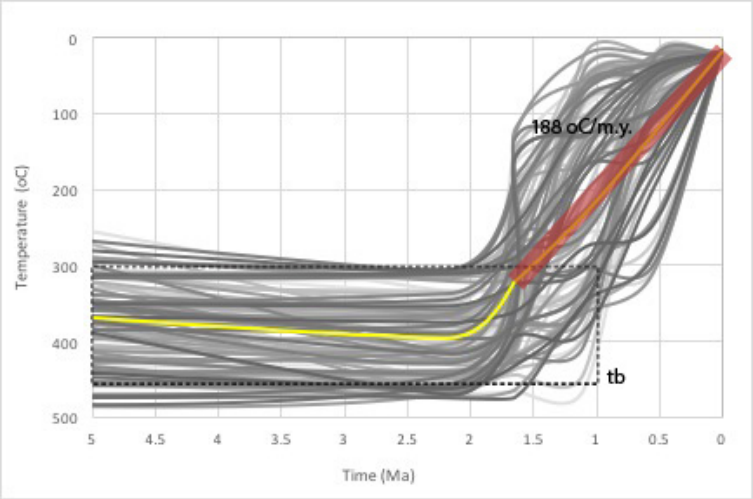

Figure 14. Time-temperature model result of ZHe for TWTP-002 at elevation of 1500m. The model focuses on one stage of accelerating cooling history in the last 1 Ma due to lack of constraint from ZFT age. The cooling rates are 188 °C/m.y. from 1 Ma to present.

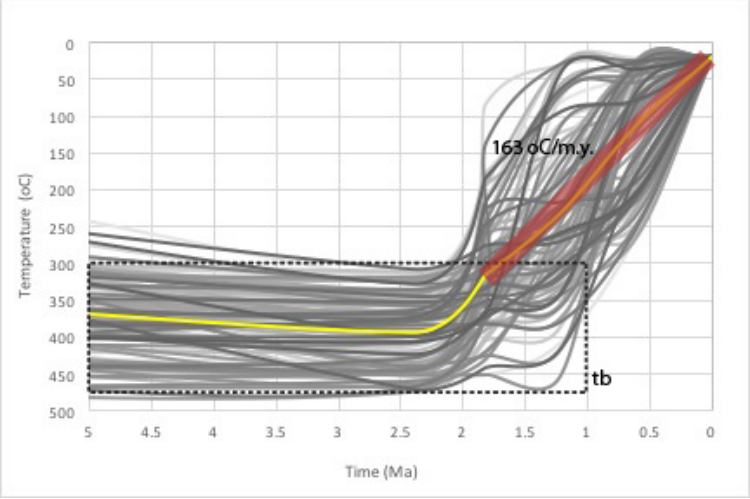

Figure 15. Time-temperature model result of ZHe for TWTP-004 at elevation of 2031m. The model focuses on one stage of accelerating cooling history in the last 1 Ma due to lack of constraint from ZFT age. The cooling rates are 163 °C/m.y. from 1 Ma to present.

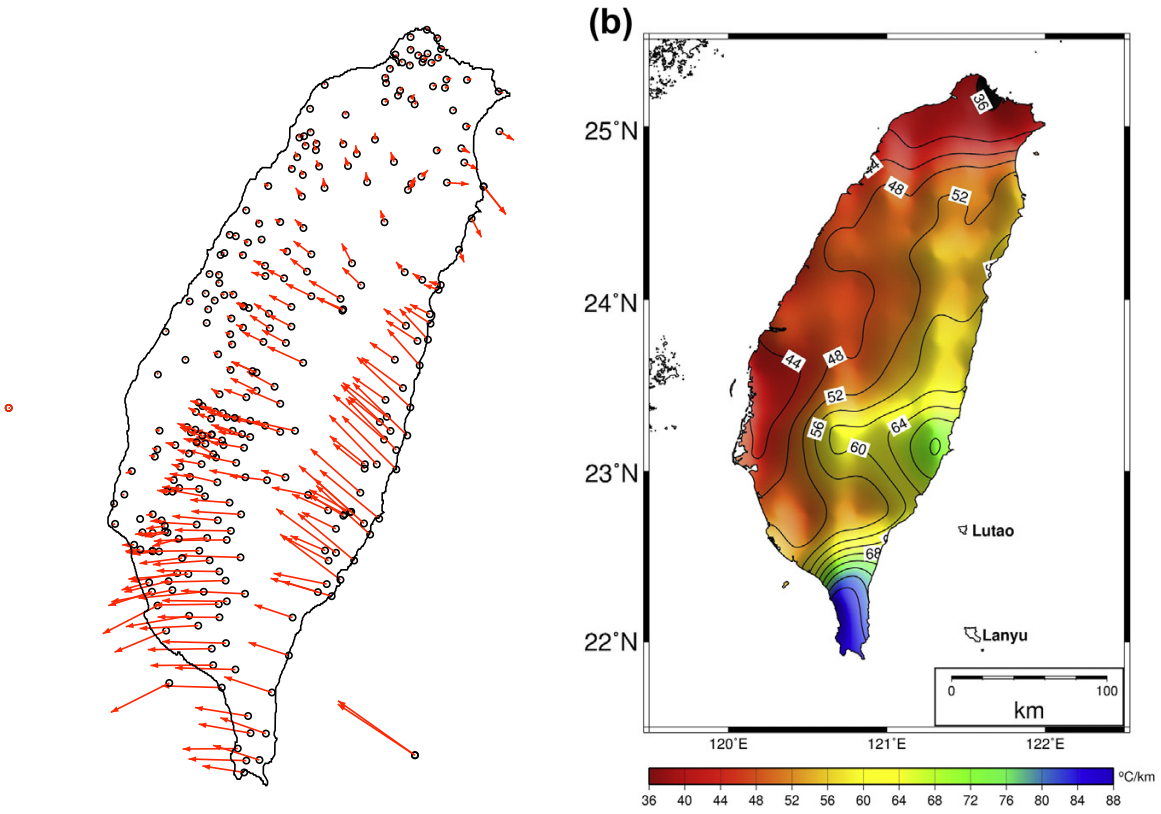

Figure 16. Displacement velocities from GPS survey (Ching et al., 2011) and map of thermal gradients map derived from Curie point depth (Curie temperature 580°C) (From Hsieh et al. (2014)). The thermal gradient of 55 °C/km is used for the study in northern Central Range.

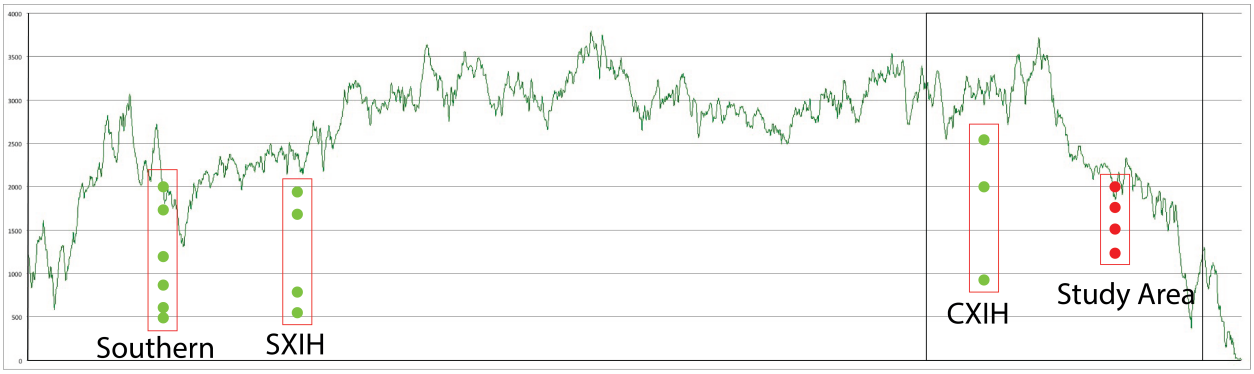

Figure 17. The topographic cross section along strike of Central Range and the locations of four age-elevation transects. The black box is used to demonstrate the exhumation models for northern Central Range shown in figure 20.

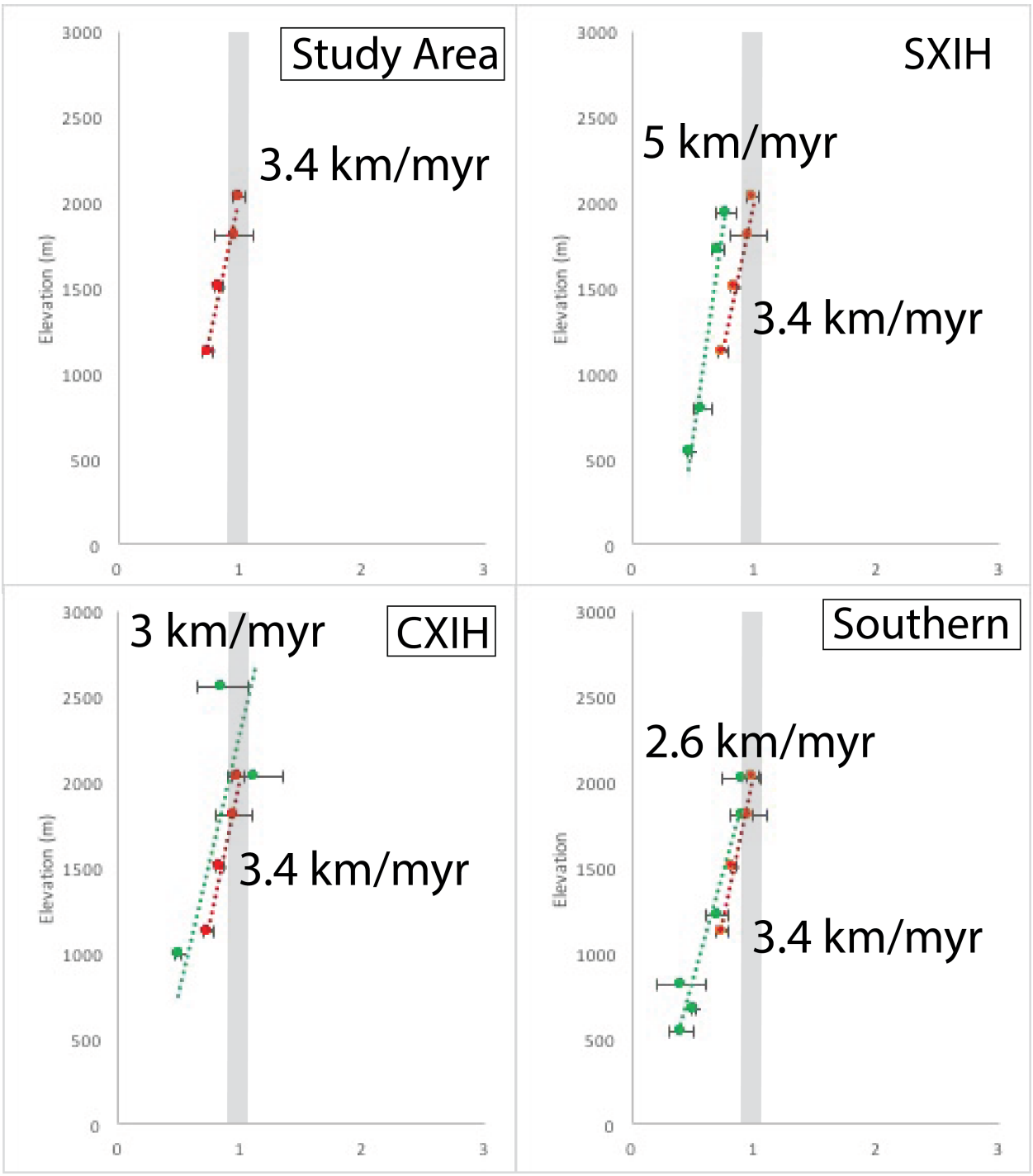

Figure 18. Comparison of four age-elevation profiles from four sites shown in figure 1. Red data and best fit – ZHe data from this study. Same data plotted in each figure for comparison. Green data and best fits – the ZHe data from Hsu et al. (2015).

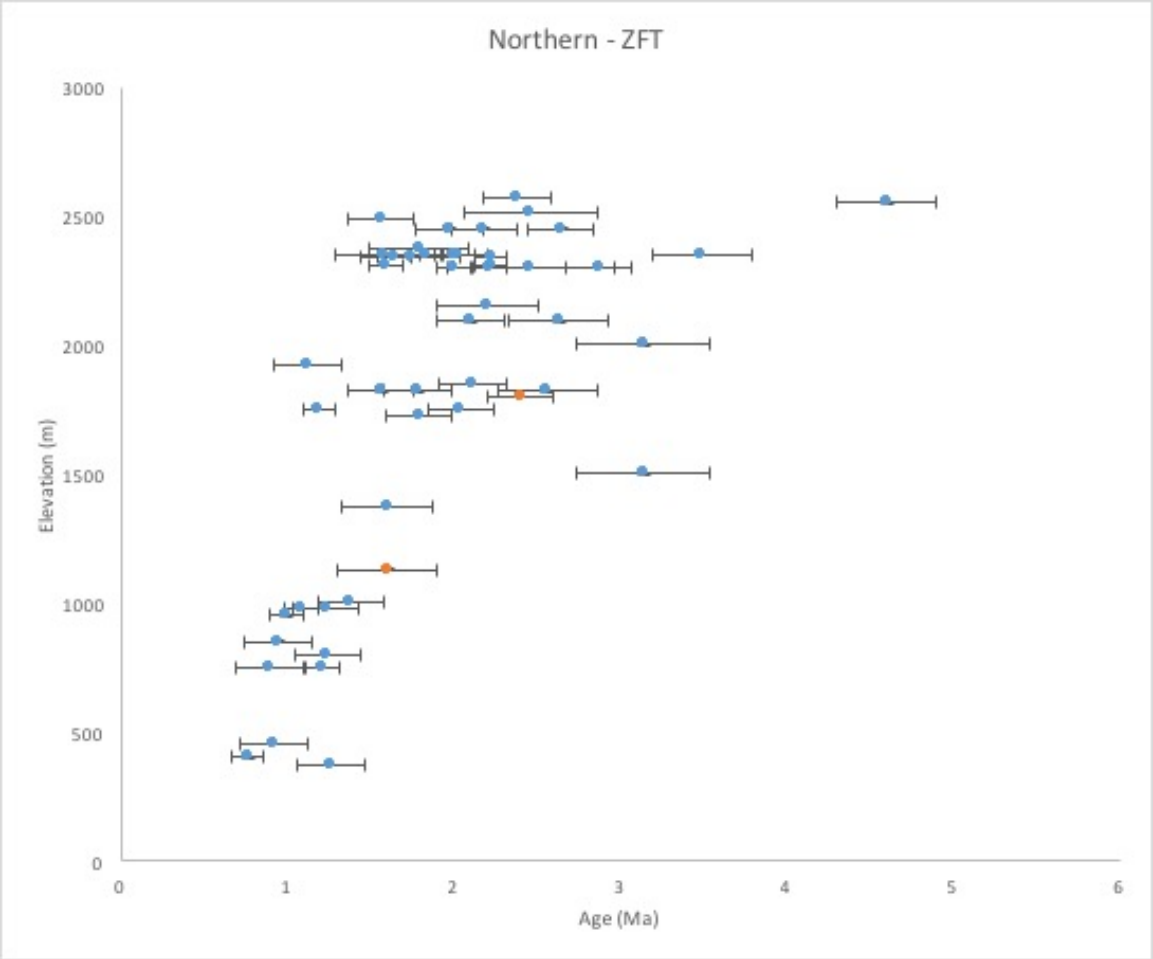

Figure 19. Comparison of ZFT data in CXIH and the study area. Orange - ZFT data from this study. Blue data - ZFT data from Tsao et al. (1996).

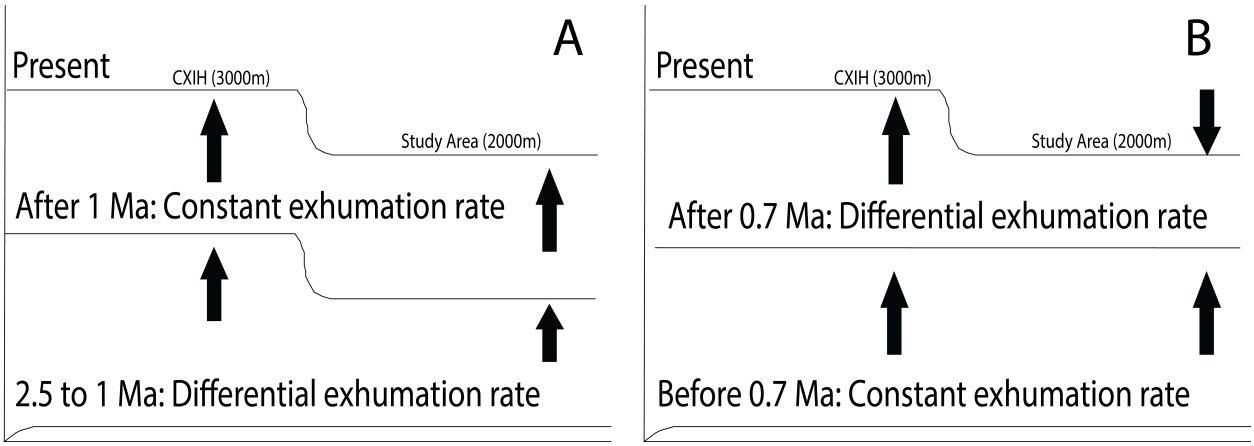

Figure 20. Hypotheses for explaining elevation offset between the study area (2000m) and CXIH (3000m): A) differential uplift and exhumation in north and south before 1 Ma; and B) differential uplift and exhumation in north and south after 0.7 Ma.

TABLES

Table 1. Zircon (U-Th)/He data obtained along Mt. Taiping in northern Central Range

Sample	Rep.	Longitude	Latitude	Elevation (m)	[U] pmol	1s pmol
Whe 1129	z001	121.507	24.409	1129	4.644	0.037
	z002				3.232	0.026
	z003				2.362	0.035
	z004				1.498	0.015
	z005				0.961	0.009
	mean					
TWTP-002	z001	121.609	24.493	1500	12.939	0.105
	z002				1.953	0.016
	z003				*9.028*	*0.072*
	z004				*1.891*	*0.016*
	z005				5.060	0.040
	mean					
TWTP-001	z001	121.601	24.503	1800	10.244	0.091
	z002				1.463	0.012
	z003				13.296	0.102
	z004				*6.773*	*0.057*
	z005				7.732	0.063
	mean					
TWTP-004	z001	121.600	24.518	2031	4.671	0.038
	z002				3.535	0.030
	z003				7.554	0.061
	z004				*11.891*	*0.093*
	z005				10.225	0.083
	mean					

Table 1. (continued)

Sample	Rep.	[Th] pmol	1s pmol	[He] pmol	1s pmol	Th/238U
Whe 1129	z001	2.590	0.013	0.00358	0.00005	0.56
	z002	1.648	0.010	0.00224	0.00006	0.51
	z003	1.689	0.019	0.00191	0.00007	0.71
	z004	1.541	0.007	0.00112	0.00005	1.03
	z005	1.045	0.005	0.00089	0.00004	1.09
	mean					
TWTP-002	z001	9.292	0.067	0.01282	0.00027	0.718
	z002	0.988	0.006	0.00174	0.00009	0.506
	z003	*7.483*	*0.033*	*0.01265*	*0.00025*	*0.829*
	z004	*1.120*	*0.007*	*0.00144*	*0.00008*	*0.592*
	z005	3.005	0.015	0.00483	0.00017	0.594
	mean					
TWTP-001	z001	5.214	0.027	0.01041	0.00018	0.51
	z002	0.829	0.005	0.00140	0.00005	0.57
	z003	7.972	0.038	0.01471	0.00023	0.60
	z004	*6.228*	*0.034*	*0.01153*	*0.00019*	*0.92*
	z005	3.939	0.025	0.00755	0.00011	0.51
	mean					
TWTP-004	z001	2.981	0.015	0.00526	0.00009	0.638
	z002	2.701	0.013	0.00386	0.00008	0.764
	z003	3.583	0.017	0.00879	0.00011	0.474
	z004	*2.158*	*0.013*	*0.01786*	*0.00036*	*0.181*
	z005	6.204	0.036	0.01101	0.00021	0.607
	mean					

Table 1. (continued)

Sample	Rep.	Raw Age Ma	1s Ma	Mean l µm	Mean r µm	Mean Ft
Whe 1129	z001	0.530	0.008	173.0	33.8	0.712
	z002	0.479	0.013	150.3	32.1	0.694
	z003	0.537	0.021	148.5	48.0	0.739
	z004	0.467	0.022	175.8	30.7	0.686
	z005	0.571	0.023	139.6	30.9	0.652
	mean					
TWTP-002	z001	0.659	0.015	208.5	48.2	0.799
	z002	0.619	0.031	136.5	36.6	0.721
	z003	*0.912*	*0.019*	*224.9*	*44.1*	*0.789*
	z004	*0.520*	*0.030*	*144.1*	*32.7*	*0.686*
	z005	0.651	0.024	198.1	36.6	0.767
	mean					
TWTP-001	z001	5.214	0.027	0.01041	0.00018	0.51
	z002	0.829	0.005	0.00140	0.00005	0.57
	z003	7.972	0.038	0.01471	0.00023	0.60
	z004	*6.228*	*0.034*	*0.01153*	*0.00019*	*0.92*
	z005	3.939	0.025	0.00755	0.00011	0.51
	mean					
TWTP-004	z001	0.760	0.014	209.8	39.4	0.777
	z002	0.719	0.016	188.6	43.5	0.779
	z003	0.812	0.012	152.4	49.5	0.783
	z004	*1.116*	*0.024*	*185.0*	*51.4*	*0.800*
	z005	0.732	0.015	160.2	42.4	0.761
	mean					

Table 1. (continued)

Sample	Rep.	Elevation (m)	Age Ft corrected Ma	2s Ma	WM Age Ma	2s Ma
Whe 1129	z001	1129	0.744	0.023		
	z002		0.691	0.038		
	z003		0.727	0.057		
	z004		0.681	0.064		
	z005		0.876	0.072		
	mean				**0.734**	**0.043**
TWTP-002	z001	1500	0.825	0.037		
	z002		0.858	0.086		
	z003		*1.156*	*0.049*		
	z004		*0.758*	*0.086*		
	z005		0.849	0.063		
	mean				**0.826**	**0.028**
TWTP-001	z001	1800	0.925	0.036		
	z002		0.849	0.061		
	z003		0.954	0.032		
	z004		*1.367*	*0.049*		
	z005		0.848	0.027		
	mean				**0.949**	**0.154**
TWTP-004	z001	2031	0.978	0.035		
	z002		0.923	0.042		
	z003		1.037	0.030		
	z004		*1.395*	*0.060*		
	z005		0.961	0.039		
	mean				**0.985**	**0.049**

For each sample, sample position (WGS84 system) and elevation (m) are given. For each replicate, I provide concentrations in U, Th and He, mass of the grain, Ft, mean radius and mean length, and raw and corrected ages.
The grains labeled in italic and underline were excluded for weighted mean age.

Table 2. Zircon Fission Track data obtained along Mt. Taiping in northern Central Range

Sample	Longitude	Latitude	Elevation (m)	Zeta	Crystal	RhoS	(Ns)	RhoI	(Ni)
Whe1129	121.507	24.409	1129	28.66	10	1.711	32	16.203	303
TWTP-001	121.601	24.503	1800	28.66	28	3.489	226	21.363	1384

Table 2. (continued)

Sample	RhoD	(Nd)	Pooled Age	± 1s	Mean Age	± 1s	Central Age	± 1s
Whe1129	10.33	4798	1.6	0.3	1.9	0.3	1.6	0.3
TWTP-001	10.33	4798	2.4	0.2	2.4	0.2	2.4	0.2

Table 3. Estimation of exhumation rates

ZHe

Sample	Elevation m	Weight mean ages m.y. (± 2σ)	Cooling rate (Tc_{ZHe} - Ts)* °C/m.y. (± 2σ)	Exhumation rate*** km/m.y. (± 2σ)
Whe1129	1129	0.734 ± 0.043	222.75 ± 21.45	4.05 ± 0.39
TWTP-002	1500	0.826 ± 0.028	197.94 ± 16.55	3.60 ± 0.30
TWTP-001	1800	0.949 ± 0.154	172.29 ± 30.91	3.13 ± 0.56
TWTP-004	2031	0.985 ± 0.049	165.99 ± 15.14	3.02 ± 0.28

ZFT

Sample	Elevation m	Weight mean ages m.y. (± 2σ)	Cooling rate (Tc_{ZFT} - Tc_{ZHe})** °C/m.y. (± 2σ)	Exhumation rate*** km/m.y. (± 2σ)
Whe1129	1129	1.6 ± 0.3	32.19 ± 27.24	0.59 ± 0.50
TWTP-001	1800	2.4 ± 0.2	21.46 ± 17.80	0.39 ± 0.32

* The closure temperature of zircon (U-Th)/He (183±13°C) to the present surface temperature (20°C)

** The closure temperature of zircon fission track (235±30°C) to the closure temperature of zircon (U-Th)/He (183±13°C)

*** The thermal gradient of 55 °C/km is used for exhumation calculation

Table. 4 Estimation of exhumation rates from HeFTy model results

Sample	Elevation m	Cooling rate stage 1 oC/m.y.	Exhumation rate km/m.y.	Cooling rate stage 2 oC/m.y.	Exhumation rate* km/m.y.
Whe1129	1129	68	1.24	256	4.65
TWTP-002	1500			188	3.42
TWTP-001	1800	68	1.24	196	3.56
TWTP-004	2031			163	2.96

* The thermal gradient of 55 °C/km is used for exhumation calculation

References

Beyssac, O., Simoes, M., Avouac, J. P., Farley, K. A., Chen, Y. G., Chan, Y. C., and Goffe, B., 2007, Late Cenozoic metamorphic evolution and exhumation of Taiwan: Tectonics, v. 26, no. 6, p. 32.

Byrne, T., and Liu, C.-S., 2002b, Preface: introduction to the geology and geophysics of Taiwan. In: Byrne T, Liu C-S (eds) Geology and geophysics of an arc-continent collision, Taiwan,: Geological Society of America Special Paper. Geological Society of America, Boulder, CO, v. 358, p. v-vii.

Chang, C.-L., and Hsu, W.-H., 2011, Discussion on the distribution of large foraminifera in the Slate Belt of Taiwan: Special Publication of the Central Geological Survey, no. 25, p. 111-132.

Chen, Y.-C., Chang, K.-T., Lee, H.-Y., and Chiang, S.-H., 2015, Average landslide erosion rate at the watershed scale in southern Taiwan estimated from magnitude and frequency of rainfall: Geomorphology, v. 228, p. 756-764.

Ching, K.-E., Hsieh, M.-L., Johnson, K. M., Chen, K.-H., Rau, R.-J., and Yang, M., 2011, Modern vertical deformation rates and mountain building in Taiwan from precise leveling and continuous GPS observations, 2000-2008: Journal of Geophysical Research. B. Solid Earth, v. 116, no. B08.

Chuang, R. Y., Johnson, K. M., Kuo, Y.-T., Wu, Y.-M., Chang, C.-H., and Kuo, L.-C., 2014, Active back thrust in the eastern Taiwan suture revealed by the 2013 Rueisuei earthquake; evidence for a doubly vergent orogenic wedge?: Geophysical Research Letters, v. 41, no. 10, p. 3464-3470.

Dadson, S., Hovius, N., Chen, H. G., Dade, W. B., Hsieh, M. L., Willett, S., and Lin, J. C., 2003, Links between erosion, runoff variability and seismicity in the Taiwan orogen: Nature, v. 426(6967), p. 648-651.

Derrieux, F., Siame, L. L., Bourlès, D. L., Chen, R.-F., Braucher, R., Léanni, L., Lee, J.-C., Chu, H.-T., and Byrne, T. B., 2014, How fast is the denudation of the Taiwan mountain belt? Perspectives from in situ cosmogenic 10Be: Journal of Asian Earth Sciences, v. 88, p. 230-245.

Farley, K. A., 2002, (U-Th)/He dating; techniques, calibrations, and applications: Reviews in Mineralogy and Geochemistry, v. 47, p. 819-843.

Farley, K. A., Wolf, R., and Silver, L. t., 1996, The effects of long alpha-stopping distances on (U-Th)/He chronometry: Geochimica et Cosmochimica Acta, v. 60, p. 4223-4229.

Fuller, C. W., Willett, S. D., Fisher, D., and Lu, C. Y., 2006, A thermomechanical wedge model of Taiwan constrained by fission-track thermochronometry: Tectonophysics, v. 425, no. 1-4, p. 1-24.

Fuller, C. W., Willett, S. D., Hovius, N., and Slingerland, R., 2003, Erosion rates for Taiwan mountain basins: New determinations from suspended sediment records and a stochastic model of their temporal variation: Journal of Geology, v. 111, no. 1, p. 71-87.

Guenthner, W. R., Reiners, P. W., Ketcham, R. A., Nasdala, L., and Giester, G., 2013, Helium diffusion in natural zircon; radiation damage, anisotropy, and the interpretation of zircon (U-Th)/He thermochronology: American Journal of Science, v. 313, no. 3, p. 145-198.

Ho, C. S., 1986, A SYNTHESIS OF THE GEOLOGIC EVOLUTION OF TAIWAN: Tectonophysics, v. 125, no. 1-3, p. 1-16.
-, 1988, An Introduction to the Geology of Taiwan: Central Geological Survey, Taiwan.
Hourigan, J. K., Reiners, P. W., and Brandon, M., 2005, U-Th zonation-dependent alpha-ejection in (U-Th)/He chronometry: Geochimica et Cosmochimica Acta, v. 46, p. 637-649.
Hourigan, M. L., McKinnon, N. B., Johnson, M., Rice, C. L., Stashuk, D. W., and Doherty, T. J., 2015, Increased motor unit potential shape variability across consecutive motor unit discharges in the tibialis anterior and vastus medialis muscles of healthy older subjects: Clin Neurophysiol, v. 126, no. 12, p. 2381-2389.
Hsieh, H.-H., Chen, C.-H., Lin, P.-Y., and Yen, H.-Y., 2014, Curie point depth from spectral analysis of magnetic data in Taiwan: Journal of Asian Earth Sciences, v. 90, p. 26-33.
Hsu, W.-H., Byrne, T. B., Ouimet, W., Lee, Y.-H., Chen, Y.-G., Soest, M. v., and Hodges, K., 2016, Pleistocene onset of rapid, punctuated exhumation in the eastern Central Range of the Taiwan orogenic belt: Geology, v. 44, no. 9, p. 719-722.
Huang, C.-Y., Chien, C.-W., Yao, B., and Chang, C.-P., 2008, The Lichi Melange; a collision melange formation along early arcward backthrusts during fore-arc basin closure, Taiwan arc-continent collision: Special Paper - Geological Society of America, v. 436, p. 127-154.
Huang, R. T. C., Wahn, K., Klenk, H.-D., and Rott, R., 1890a, Fussion of liposomes containing the glycoproteins of influenza virus with tissue culture cells: Virology, v. 104, p. 294-302.
Hurford, A. J., and Green, P. F., 1982, A user's guide to fission track dating calibration.: Earth Planet. Sci. Lett., v. 59, p. 343-354.
Jahn, B. M., Martineau, F., Peucat, J. J., and Cornichet, J., 1986, GEOCHRONOLOGY OF THE TANANAO SCHIST COMPLEX, TAIWAN, AND ITS REGIONAL TECTONIC SIGNIFICANCE: Tectonophysics, v. 125, no. 1-3, p. 103-124.
Juang, W.-S., Bellon, H., and Anonymous, 1986, Potassium-argon ages of the Tananao Schist in Taiwan: Chung Kuo Ti Ch'ih Hsueh Hui Chuan Kan = Memoir of the Geological Society of China, v. 7, p. 405-416.
Ketcham, R. A., 2005, Forward and Inverse Modeling of Low-Temperature Thermochronometry Data: Reviews in Mineralogy and Geochemistry, v. 58, no. 1, p. 275.
Lee, C. S., and Lee, C.-I., 1977, A Brief Introduction To Taiwan Paleogene Larger Foraminifers And Their Distribution: Mining Technology, v. 15, no. 4, p. 146-161.
Lee, Y.-H., Byrne, T., Wang, W.-H., Lo, W., Rau, R.-J., and Lu, H.-Y., 2015, Simultaneous mountain building in the Taiwan orogenic belt: Geology (Boulder), v. 43, no. 5, p. 451-454.
Lee, Y. H., Chen, C. C., Liu, T. K., Ho, H. C., Lu, H. Y., and Lo, W., 2006, Mountain building mechanisms in the Southern Central Range of the Taiwan Orogenic Belt - From accretionary wedge deformation to arc-continental collision: Earth and Planetary Science Letters, v. 252, no. 3-4, p. 413-422.
Lin, A. T., Watts, A. B., and Hesselbo, S. P., 2003, Cenozoic stratigraphy and subsidence history of the South China Sea margin in the Taiwan region: Basin Research, v. 15, no. 4, p. 453-478.
Liu, T. K., Hsieh, S., Chen, Y. G., and Chen, W. S., 2001, Thermo-kinematic evolution of the Taiwan oblique-collision mountain belt as revealed by zircon fission track dating: Earth and Planetary Science Letters, v. 186, no. 1, p. 45-56.

Ludwig, K. R., 2003, Mathematical-statistical treatment of data and errors for (super 230) Th/U geochronology: Reviews in Mineralogy and Geochemistry, v. 52, p. 631-656.
Mancktelow, N. S., and Grasemann, B., 1997, Time-dependent effects of heat advection and topography on cooling histories during erosion: Tectonophysics, v. 270, no. 3–4, p. 167-195.
Murakami, M., and Svojika, M., 2007, Zircon fission-track technique: a laboratory procedure adopted at the Institute of Geology: Academy of Sciences of the Czech republic, v.v.i. Fission Track News Letters,, v. 20, p. 13-19.
Naeser, C. W., 1967, The use of apatite and sphene for fission track age determinations: Bull. Geol. Soc. Amer., v. 78, 1523.
Ouimet, W. B., Byrne, T. B., Huang, C., Bierman, P. R., Lee, Y. H., Hsu, W. H., Hsieh, M. L., Van Soest, M. C., and Anonymous, 2015, Extreme landscape disequilibrium and slow erosion during rapid mountain building: American Geophysical Union Fall Meeting, v. 2015, p. Abstract T32B-02.
Price, P. B., and Walker, R. M., 1963, Fossil Tracks of Charges Particles in Mica and the Age of Minerals: J. Geophs. Res., v. 68, 4,847.
Reiners, P. W., 2005, Zircon (U-Th)/He Thermochronometry: Reviews in Mineralogy and Geochemistry, v. 58, no. 1, p. 151.
Reiners, P. W., and Brandon, M. T., 2006, Using thermochronology to understand orogenic erosion: Annual Review of Earth and Planetary Sciences, v. 34, p. 419-466.
Reiners, P. W., Farley, K. A., and Hickes, H. J., 2002, He diffusion and (U–Th)/He thermochronometry of zircon: initial results from Fish Canyon Tuff and Gold Butte: Tectonophysics, v. 349, no. 1–4, p. 297-308.
Reiners, P. W., Spell, T. L., Nicolescu, S., and Zanetti, K. A., 2004, Zircon (U-Th)/He thermochronometry: He diffusion and comparisons with 40Ar/39Ar dating: Geochimica et Cosmochimica Acta, v. 68, no. 8, p. 1857-1887.
Rezaeian, M., 2008, Coupled tectonics, erosion and climate in the Alborz Mountains, Iran: PhD thesis, University of Cambridge, p. 219.
Simoes, M., and Avouac, J. P., 2006, Investigating the kinematics of mountain building in Taiwan from the spatiotemporal evolution of the foreland basin and western foothills: Journal of Geophysical Research-Solid Earth, v. 111, no. B10, p. 25.
Stanley, R. S., Hill, L. B., Chang, H. C., and Hu, H. N., 1981, A cross-section through the southern central mountains of Taiwan: Mem. Geol. Soc. China, v. 4, p. 443-474.
Stuewe, K., White, L., and Brown, R., 1994, The influence of eroding topography on steady-state isotherms; application to fission track analysis: Earth and Planetary Science Letters, v. 124, no. 1-4, p. 63-74.
Suppe, J., 1981, Mechanics of mountain building and metamorphism in Taiwan: Memoir Geol Soc China, v. 4, p. 67–89.
-, 1984, Kinematics of arc-continent collision, flipping of subduction, and back-arc spreading near Taiwan: Geological Society of China Memoir, v. 6, p. 131-146.
Teng, L. S., 1990, GEOTECTONIC EVOLUTION OF LATE CENOZOIC ARC CONTINENT COLLISION IN TAIWAN: Tectonophysics, v. 183, no. 1-4, p. 57-76.

Teng, L. S., Chen, W. S., Wang, Y., Song, S. R., and Lo, H. J., 1988, Toward a comprehensive stratigraphic system of the Coastal Range, eastern Taiwan: Acta Geologica Taiwanica, v. 26, p. 13-36.

Teng, L. S., and Wang, Y., 1981, Island arc system of the Coastal Range, eastern Taiwan: Proceedings of the Geological Society of China, v. 24, p. 99-112.

Tillman, K. S., and Byrne, T. B., 1995, KINEMATIC ANALYSIS OF THE TAIWAN SLATE BELT: Tectonics, v. 14, no. 2, p. 322-341.

Tsan, S. F., 1977, Remarks on the Suao section of the Central Range of Taiwan: Mem. Geol. Soc. China, v. 2, p. 141-145.

Tsao, S.-J., 1996, The geological significance of illite critallinity zircon fission-track ages and K-Ar ages of metasedimentary rocks of the Central Range: National Taiwan University, Taipei, ROC.

van Soest, M. C., Hodges, K. V., Wartho, J.-A., Biren, M. B., Monteleone, B. D., Ramezani, J., Spray, J. G., and Thompson, L. M., 2011, (U-Th)/He dating of terrestrial impact structures: The Manicouagan example: Geochemistry, Geophysics, Geosystems, v. 12, no. 5, p. n/a-n/a.

Wendt, I., and Carl, C., 1991, The statistical distribution of the mean squared weighted deviation: Chemical Geology: Isotope Geoscience Section, v. 86, no. 4, p. 275-285.

Whipple, K. X., DiBiase, R. A., Ouimet, W. B., and Forte, A. M., 2016, Preservation or piracy: Diagnosing low-relief, high-elevation surface formation mechanisms: Geology, v. 45, no. 1, p. 91.

Wintsch, R. P., Yeh, M. W., and Anonymous, 2011, Lower greenschist facies oscillations across the brittle-ductile transition induced by alternating reaction softening and hardening events: American Geophysical Union Fall Meeting, v. 2011, p. Abstract T41C-08.

Wolf, C. M., Griffith, B., Reed, C., and Temple, S. A., 1996, Avian and Mammalian Translocations: Update and Reanalysis of 1987 Survey Data

Translocaciones de Aves y Mamíferos: Actualizaceón y Re-análisis de Datos Generados: Conservation Biology, v. 10, no. 4, p. 1142-1154.

Wu, F. T., 1978, RECENT TECTONICS OF TAIWAN: Journal of Physics of the Earth, v. 26, no. Supplement, p. S265-S299.

Wu, F. T., Kuo-Chen, H., and McIntosh, K. D., 2014, Subsurface imaging, TAIGER experiments and tectonic models of Taiwan: Journal of Asian Earth Sciences, v. 90, p. 173-208.

Wu, J.-C., Yang, K.-M., Chen, Y.-R., and Chi, W.-R., 2011, Tectonic implications of stratigraphy architecture in distal part of foreland basin, southwestern Taiwan: in Closson, D., ed., Tec- tonics: Rijeka, Croatia, InTech, p. p. 171–198.

Yaba, H., and Hanzawa , S., 1930, Stratigraphy of Tertiary foraminiferal rocks of Taiwan: Geol. Papers for the Memory of Dr. T. Ogawa's 61th Birthday p. 83-126, Ko-bundo, Tokyo.

Yu, S. B., Chen, H. Y., and Kuo, L. C., 1997, Velocity field of GPS stations in the Taiwan area: Tectonophysics, v. 274, no. 1-3, p. 41-59.